Catalyst development for carbon neutral liquid fuel production from carbon dioxide

二酸化炭素からのカーボンニュートラル液体燃料製造用触媒の開発

Heng Zhao

趙 恒

Supervisor: Prof. Noritatsu Tsubaki

Tsubaki Laboratory

Graduate School of Science and Engineering

University of Toyama

Preface

In the past decades, severe climate deterioration has been induced by massive emissions of carbon dioxide (CO_2). Trapping, storing and reutilizing CO_2 emissions from industry is needed urgently to achieve global carbon neutrality. With the development of industrialization, cars, trucks and airplanes, liquid fuel is indispensable in human life. Converting CO_2 into carbon neutral liquid fuel (C_{5+} hydrocarbons) is an essential way to relieve rapid consumption of fossil fuels and high demands for carbon-based energy resources at the same time. However, the low CO_2 conversion of photocatalysis and the short chain of the products from electrocatalysis limited their large-scale utilization. Compared to photocatalysis and electrocatalysis, which are still in the development stage, thermocatalytic hydrogenation of CO_2 has been widely studied and commercialized due to the ultra-high efficiency and well controllability of target products.

Generally, thermocatalytic hydrogenation of CO_2 generally occurs via a methanol-mediated route (MeOH route) or a CO_2 modified Fischer-Tropsch synthesis (CO_2-FTS) mechanism. For the MeOH route, CO_2 is first hydrogenated to methanol (MeOH). The MeOH then is converted to hydrocarbons via some dehydration and/or coupling reactions. Unfortunately, the catalysts for the MeOH route are expensive and the reaction process is complicated. In the case of CO_2-FTS route, CO_2 is first reduced to carbon monoxide (CO) by reverse water gas shift (RWGS) reaction through two widely recognized mechanisms. The first mechanism is a redox mechanism, in which CO_2 is reduced by catalysts to form CO and the catalysts subsequently be reduced to produce water (H_2O). The second one is a formate-intermediate mechanism, in which CO_2 reacts with hydrogen (H_2) directly to form formate, followed by further hydrogenation to produce CO and H_2O. After the RWGS reaction, hydrocarbons can be produced by FTS reaction. Similarly, two possible mechanisms, including direct CO dissociation mechanism and H-assisted CO dissociation mechanism, for the FTS rection are widely reported. In the direct CO dissociation mechanism, CO is first adsorbed and dissociated

to *C and *O on catalyst. Then, *CH_x intermediate species are formed by the reaction of dissociated surface carbon with adsorbed surface hydrogen atoms. Simultaneously, dissociated *O is removed by reacting with adsorbed *H and *CO to produce H_2O and CO_2, respectively. Finally, *CH_x intermediate species are further coupled and/or hydrogenated into hydrocarbons. As for the H-assisted CO dissociation mechanism, FTS reaction occurs via the following elementary steps: (1) *CO reacts with *H to form formyl (*HCO) intermediates and subsequently be further hydrogenated to hydroxymethylene (*HCOH) intermediates; (2) *HCOH is dissociated to *OH and *CH that ultimately form H_2O and monomers (*CH_2), respectively; (3) coupling, hydrogenation and dehydrogenation of *CH_2 into paraffins and olefins as products.

As a big challenge in CO_2-FTS, researchers have been struggling in adjusting the products distribution for a high selectivity of target products. However, CO_2 hydrogenation through the CO_2-FTS route generally exhibits a broad spectrum of products that can be described as an Anderson-Schulz-Flory (ASF) model. The classical ASF model limits the maximum selectivities of hydrocarbons. For example, the selectivities of C_2-C_4 hydrocarbons, gasoline (C_5-C_{11}), jet fuel (C_8-C_{16}) and diesel (C_{10}-C_{20}) are restricted by 58 %, 48 %, 41 % and 40 %, respectively. Therefore, my work focuses on developing novel catalysts to break the limitation of the ASF model and thus increase the yield of carbon neutral liquid fuel.

According to the reaction process of CO_2-FTS, both RWGS reaction and FTS reaction play important roles in CO_2 hydrogenation. In chapter 1, multi-promoters, including potassium, manganese and titanium, were incorporated into iron catalyst for improving CO_2 hydrogenation and the influences of each promoter were investigated in detail. Besides, the content of each component was optimized to achieve a well-matching tandem catalysis performance between RWGS reaction and FTS reaction. The results showed that the introduction of potassium could improve the RWGS reaction and chain growth capacity by utilizing abundant oxygen vacancy and strong competitive adsorption. With the further addition of manganese, more active carbides sites with benign dispersion were detected owing to the strong interaction between

manganese and iron species. When titanium was added, the catalytic performance of the catalyst was improved by the stronger CO_2 adsorption capacity and longer resistance time of reactants. Therefore, the well-matching catalysis between RWGS and FTS was achieved on the corresponding $K_3/FeMn_{10}Ti_{20}$ catalyst, achieving C_{5+} yield as high as 1282.7 $g_{fuel}kg_{cat}^{-1}h^{-1}$ at a CO_2 conversion of 44.9 % and maintaining a rather low by-products selectivity (9.6 % for CO, 12.8 % for CH_4).

Recently, the combination of CO_2-FTS catalysts with solid acidic catalysts, especially zeolites are extensively investigated for optimizing the products selectivity in CO_2 hydrogenation. In chapter 2, a bifunctional catalyst composed of K-Fe/C and ZSM-5 zeolite was developed and it was found to be efficiency in the production of carbon neutral liquid fuel via simply tuning the microenvironment properties of ZSM-5 zeolite. The catalysts were characterized by various methods, such as Brunauer-Emmett-Teller (BET), transmission electron microscopy (TEM), X-ray diffractometer (XRD), temperature programmed desorption (NH_3-TPD), and X-ray photoelectron spectroscopy (XPS). K-Fe/C catalyst was mainly responsible for the formation of olefins, while ZSM-5 catalyst was mainly responsible for olefin secondary reaction, such as aromatization, isomerization, and cracking reaction. Surface acid properties of ZSM-5 were well regulated through different ion-exchange strategies, in which the strong surface acid properties of ZSM-5 were eliminated with the utilization of K^+-ion exchange strategy and then it presented a high C_{5+} selectivity by suppressing the light saturated hydrocarbons formation.

Herein, two highly efficient catalysts were rationally designed and successfully synthesized for the production of carbon neutral liquid fuels from CO_2 hydrogenation via the CO_2-FTS route. This work provides new insights into the realization of global carbon neutrality by reutilizing of CO_2.

Contents

Chapter 1

Multi-promoters regulated iron catalyst with well-matching reverse water-gas shift and chain propagation for boosting CO_2 hydrogenation

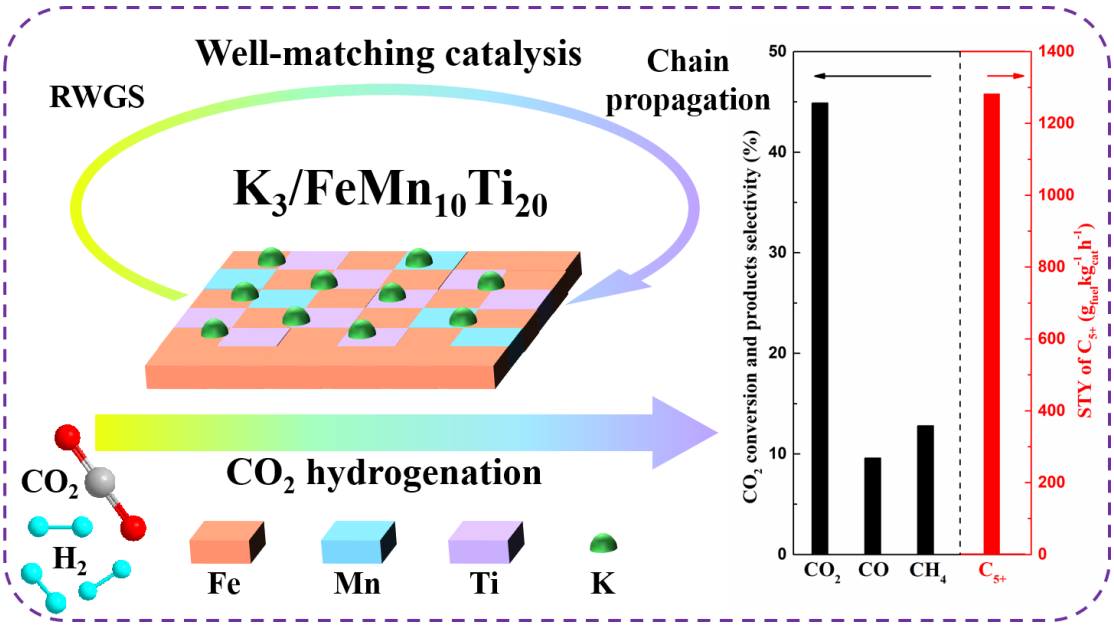

The well-matching catalysis between reverse water gas shift (RWGS) reaction and chain propagation in CO_2 hydrogenation was achieved on the corresponding $K_3/FeMn_{10}Ti_{20}$ catalyst, achieving C_{5+} yield as high as 1282.7 $g_{fuel}kg_{cat}^{-1}h^{-1}$ at CO_2 conversion of 44.9 % and maintaining a rather low by-products selectivity (9.6 % for CO, 12.8 % for CH_4).

Abstract

In chapter 1, multi-promoters, including potassium, manganese and titanium, were incorporated into iron catalyst for improving CO_2 hydrogenation and the influences of each promoter were investigated in detail. Besides, the content of each component was optimized to achieve a well-matching tandem catalysis performance between reverse water gas shift (RWGS) reaction and chain propagation reaction. The results showed that the introduction of potassium could improve the RWGS reaction and chain growth capacity by utilizing abundant oxygen vacancy, and strong competitive adsorption. With the further addition of manganese, more active carbides sites with benign dispersion were detected owing to the strong interaction between manganese and iron species. When titanium was added, the catalytic performance of the catalyst was improved by the stronger CO_2 adsorption capacity and longer resistance time of reactants. Therefore, the well-matching catalysis between RWGS and chain propagation was achieved on the corresponding $K_3/FeMn_{10}Ti_{20}$ catalyst, achieving C_{5+} yield as high as 1282.7 $g_{fuel}kg_{cat}^{-1}h^{-1}$ at CO_2 conversion of 44.9 % and maintaining a rather low by-products selectivity (9.6 % for CO, 12.8 % for CH_4).

Keyword: CO_2 hydrogenation; Iron-based catalyst; Liquid hydrocarbons; Promoters; Well-matching catalysis.

1.1 Introduction

Owing to the development of industrialization, the demands for carbon-based energy resources have increased rapidly, generally from non-renewable resources such as petroleum, and the corresponding massive emissions of carbon dioxide (CO_2) bring a lot of problems associating with greenhouse effect and ocean acidification. Converting CO_2 into value-added liquid fuel or chemicals by catalytic hydrogenation is an attractive route to dissolve this problem [1-3]. Generally, catalytic conversion of CO_2 contains two reactions as follow: CO_2 is first reduced to CO by reverse water gas shift (RWGS) reaction (Eq. (1.1)) and subsequently be hydrogenated to hydrocarbons via Fischer-Tropsch synthesis (FTS, Eq. (1.2)) [4,5]. Obviously, the well-matching catalysis between RWGS and chain propagation could lead to an improved catalytic result.

$$CO_2 + H_2 \rightarrow CO + H_2O \qquad \Delta_r H_{573\,K} = +38\,kJ/mol \qquad (1.1)$$

$$nCO + 2nH_2 \rightarrow C_nH_{2n} + nH_2O \qquad \Delta_r H_{573\,K} = -166\,kJ/mol \qquad (1.2)$$

Among these active metals using for CO_2-FTS (Fe, Co, Ni, Ru and Rh), Fe has been widely utilized and considered as a promising active metal, due to its excellent catalytic activity and low cost [6]. During reaction processes, iron species can be converted into Fe_3O_4 and Fe_xC_y for RWGS and chain propagation, respectively. Unfortunately, pure Fe catalyst generally exhibits low CO_2 conversion and high selectivity of methane (CH_4) [4,7]. In order to improve the catalytic performance, many electronic/structural promoters have been introduced and investigated [8-10]. Potassium (K) is usually employed to enhance alkene selectivity and inhibit the formation of CH_4, shifting the products distribution from light hydrocarbons to heavy hydrocarbons [5]. Kim et al. [11] revealed that the addition of K promoted the formation of vacancy sites over the surface of iron oxides and carbides, leading to the production of long-chain hydrocarbons. Besides, more basicity sites committing to CO_2 molecules

adsorption, will be formed with the introduction of alkali K promoter. Apart from K, manganese (Mn) was also widely used as an electronic promoter to tailor hydrocarbons distribution. In addition to the increase of surface basicity of catalyst, it was reported that the carburization behavior of Fe species would be increased with the addition of alkali Mn [12]. Similar results reported by Ma et al. [13] demonstrated that the addition of Mn brought a negative effect to the intrinsic RWGS, due to the transformation from the RWGS-active Fe_3O_4 phase to the FTS-active Fe_5C_2 phase. Besides, Ma et al. [14] reported that Mn could greatly enhance the selectivity of light olefins and suppress the formation of undesired CH_4. Considering the complementary positive effects, both K and Mn are often doped into the Fe-based catalysts as promoters at the same time. Witoon et al. [15] studied the effect of transition metals (Cu, Mn, V, Zn or Co) on the Fe/K-Al_2O_3 catalyst and found that Fe-Mn/K/Al_2O_3 exhibited the maximum ratio of olefin/paraffin. It has been proved that light olefins can undergo secondary reactions such as reinserting of CH* species or hydrogenation, which play a crucial for increasing the selectivity of liquid hydrocarbons [16]. Although the utilization of K and Mn as promoters in Fe-based catalysts are suitable for improving CO_2 hydrogenation to liquid hydrocarbons, the catalyst still shows a relative high CO and CH_4 selectivity as reported by Fierro et al. [17] and Willauer et al. [18] to some extent, there is still room for improving catalytic performance by further matching RWGS and C-C coupling.

In this work, titanium (Ti) promoter was first incorporated into FeMnK catalysts to further accelerate the RWGS and the following chain propagation, due to its excellent CO_2 adsorption and chain propagation capacity [19,20]. Besides, the additive amount of each promoter component was also tuned to obtain the optimal value. The contribution of each promoter for the tandem reactions (RWGS and chain propagation) has also been studied by applying various characterizations. Typically, the catalyst, named as K_3/$FeMn_{10}Ti_{20}$, was modified by three promoters with optimal contents, correspondingly, this K_3/$FeMn_{10}Ti_{20}$ catalyst realized the splendid catalytic performance in the CO_2 hydrogenation by regulating the well-matching catalysis between RWGS and chain propagation.

1.2 Experiment

1.2.1 Materials

All the reagents for the preparation of catalysts were A.R. grade without any purification. Titanium (IV) oxide (TiO_2, mixture of rutile and anatase), sodium hydroxide (NaOH), hydrochloric acid (HCl), iron (III) nitrate nonahydrate ($Fe(NO)_3{\cdot}9H_2O$), manganese (II) nitrate hexahydrate ($Mn(NO_3)_2{\cdot}H_2O$), ammonium carbonate ($(NH_4)_2CO_3$) and potassium nitrate (KNO_3) were pursed from FUJIFILM Wako pure chemical corporation, Japan.

1.2.2 Catalyst preparation

Before the preparation, TiO_2 was first pretreated by alkali via a hydrothermal method. Next, Fe and Mn were coated by a coprecipitation method. Finally, K was introduced by an impregnation method. All the information about this catalyst preparation has been described detailly below.

TiO_2 was first pre-treated by NaOH via a hydrothermal method. 2 g TiO_2 was dissolved in 10 M NaOH of 70 mL solution and hydrothermally treated at 130 °C for 24 h in a Teflon-lined stainless-steel autoclave. Subsequently, the precipitate was filtered and washed with deionized water followed by 0.2 M HCl of 2 L aqueous solution until the pH reached 1 and then washed with deionized water again until the pH returned to neutral. The resulting solid was dried in air at 100 °C for 12 h and denoted as Alk-TiO_2.

$FeMnO_x$-TiO_2 catalysts were synthesized by a co-precipitation method. In a typical synthesis, a certain amount of Alk-TiO_2, $Fe(NO)_3{\cdot}9H_2O$ and $Mn(NO_3)_2{\cdot}H_2O$ was dissolved in deionized water (100 mL) with vigorously stirring and noted as solution A. Then, solution B containing 2M $(NH_4)_2CO_3$ was added into solution A drop by drop until the pH reached 9. After that, the mixtures were stirred at room temperature for 5 h. Finally, the obtained precipitate was dried in air at 120 °C for 12 h and then calcined in air at 550 °C for 5 h. The sample was denoted as FeMnTi.

K was introduced by a wet-impregnation method. A certain amount of KNO_3 was dissolved in deionized water (2 mL) and then 2 g FeMnTi was added. After ultrasound

treatment of 30 min, the mixture was dried at 60 °C for 12 h and calcined at 550 °C for 5 h in air. Before the CO_2 hydrogenation reaction, all the obtained samples were pressed into 40-60 mesh.

The final samples were denoted as $K_a/Fe_bMn_cTi_d$, in which a (0, 1, 3, 5), b (90), c (0, 5, 10, 20) and d (0, 10, 20, 30) stand for the molar ratio of each component. To be special, when the component was zero content in the catalyst, the letter representing that component did not exist in the forum and the additive amount of corresponding compound was zero during the preparation process. In addition, the symbol of b was also ignored, owing to the same content in each catalyst. In order to further study the effect of pretreatment on TiO_2, $K_3/FeMn_{10}Ti_{20}$-N was prepared by the same method, using the TiO_2 without any pretreatment.

1.2.3 Catalyst characterization

The molar ratio of each component in the $K_a/Fe_bMn_cTi_d$ catalysts was first determined by X-ray fluorescence (XRF) on a PW2404R (PHILIPS, Nederland).

The microstructure and elemental distributions on the surface of the catalysts were investigated by Field Emission Scanning Electron Microscope (FE-SEM) and Energy Dispersive Spectroscopy (EDS, JSM-IT700HR, JEOL, Japan).

The specific surface area and total pore volume were tested using an AUTOSORB-1 equipment from Quantachrome Instruments at liquid N_2 temperature (-196 °C). Prior to test, each sample was degassed at 200 °C under vacuum conditions for 6 h.

Powder X-ray diffraction (XRD) was carried out on an Ultima IV-NS (Rigaku, Japan) equipped with X-ray source of Cu-Kα. Scans were taken with a 2 theta range from 10° to 80° at a speed of 2 °/min.

An ESCALAB 250 photoelectron spectrometer (Thermo Fisher Scientific, USA) with a monochromatized microfocused Al-Kα X-ray source was used for X-ray photoelectron spectroscopy (XPS) measurements. Charge effects of the samples were corrected by setting the binding energy of adventitious carbon (C 1s) at 284.6 eV.

H_2-temperature-programmed reduction (H_2-TPR) experiments were performed on a BELCAT II-T-SP (Microtrac mrb, USA). 50 mg sample were pretreated at 300 °C in pure He of 30 mL/min flow rate for 2 h and then cooled to 100 °C. Subsequently, the

sample was reduced with an Ar gas mixture containing 5 % H_2, at a flow rate of 30 mL/min, and the temperature was increased to 900 °C at a heating rate of 10 °C/min. The consumption of H_2 was recorded by a thermal conductivity detector (TCD).

In order to clarify the surface basicity of the catalyst, CO_2 temperature-programmed desorption (CO_2-TPD) was measured at a BELCAT II-T-SP (Microtrac mrb, USA). 50 mg sample was first reduced at 400 °C in pure H_2 of 30 mL/min flow rate for 2 h. After cooling to 50 °C, pure CO_2 gas was introduced at a flow rate of 30 mL/min for 1 h, and then the physical adsorbed CO_2 molecules were removed by pure He gas at a flow rate of 30 mL/min for 1 h. Finally, the temperature was increased to 400 °C at a heating rate of 10 °C/min and the desorbed CO_2 was recorded by TCD. The peak area of CO_2 was quantitatively calibrated by employing CO_2 pulses.

1.2.4 Catalyst activity evaluation

CO_2 hydrogenation reaction was evaluated by a stainless steel fixed-bed reactor. Typically, 0.25 g catalyst diluted with 1 g of quartz granule was charged into the reactor and reduced at 400 °C for 8 h by pure H_2 flow (40 $mLmin^{-1}$, atmospheric pressure). After reduction, the reactor was cooled down to the reaction temperature and then the reactant gas mixtures including $H_2/CO_2/Ar$ (H_2: 70.00 v%, CO_2: 25.03 v%, Ar: 4.97 v%) were fed into the reactor until the pressure reached 5.0 MPa. During the CO_2 hydrogenation, the gaseous products were detected by two online gas chromatographs with thermal conductivity detector (TCD) and flame ionization detector (FID). The liquid hydrocarbons in the effluent were collected by an ice trap containing tridecane as solvent and analyzed by an offline gas chromatograph with a FID detector. CO_2 conversion (CO_2 conv.), CO selectivity (S_{CO}), hydrocarbon distributions (C_i sel., excluding CO), selectivity of oxygenated products (Oxy sel., excluding CO) and space-time yield of liquid fuels (STY of C_{5+}) were calculated using Eqs, 1.3-1.7.

$$CO_2 \text{ conv. (C-mol\%)} = \frac{CO_{2\,in} - CO_{2\,out}}{CO_{2\,in}} \times 100\% \quad (1.3)$$

$$S_{CO} \text{ (C-mol\%)} = \frac{CO_{out}}{CO_{2\,in} - CO_{2\,out}} \times 100\% \quad (1.4)$$

$$C_i \text{ sel. (C-mol\%)} = \frac{\text{Moles of } C_i \text{ hydrocarbons} \times i}{\sum_{i=1}^{n} \text{Moles of } C_i \text{ hydrocarbons} \times i + \sum_{i=1}^{n} \text{Moles of } C_i \text{ Oxygenated products} \times i} \times 100\% \quad (1.5)$$

$$\text{Oxy sel. (C-mol\%)} = \frac{\text{Moles of oxygenated products}}{\sum_{i=1}^{n} \text{Moles of } C_i \text{ hydrocarbons} \times i + \sum_{i=1}^{n} \text{Moles of } C_i \text{ Oxygenated products} \times i} \times 100\% \quad (1.6)$$

$$\text{STY of } C_{5+} \ (g_{fuels} kg_{catalyst}^{-1} h^{-1}) = 14 \times 1000 \times n_{CO_2} \times (100\% - \text{CO sel.}) \times C_{5+} \text{ sel.} \quad (1.7)$$

Herein, $CO_{2\ in}$, $CO_{2\ out}$, $CO_{\ out}$, respectively represent the mole fraction of CO_2 at the inlet, CO_2 at the outlet and CO at the outlet. Besides, 14, 1000 and n_{CO_2} represent the molar weight of CH_2 (14 g/mol), 1000 gram per kilogram and moles of CO_2 converted by per gram of catalyst per hour, respectively. The carbon balance in the reaction reached above 95 %.

1.3 Results

1.3.1 Textural properties of different catalysts

The surface compositions of the fresh catalysts were first tested by XRF and shown in Table 1.1. Clearly, the actual content of each component in all the catalysts approached the theoretical value. Besides, the morphologies of the catalysts with different promoters were tested by FE-SEM and EDS. As depicted in Fig. 1.1 and Fig. 1.2, all the catalysts were composed by nano-spherical particles. When K was loaded alone, it aggregated on the surface of the catalyst. However, this phenomenon was alleviated with the addition of Mn and Ti. Therefore, the benign dispersion of each component could be also found on the $K_3/FeMn_{10}Ti_{20}$ catalyst (Fig. 1.3A). Furthermore, in order to clarify the influence of the pretreatment on TiO_2, the textural properties of TiO_2 with or without NaOH pretreatment were investigated. With the pretreatment of NaOH, its crystalline phase was destroyed [21], and the microstructure was changed from spherical to nanowire, resulting in the smaller crystalline size and larger specific surface area (Fig. 1.4, 1.5 and Table 1.2). As a result, more TiO_2 gathered over the surface of $K_3/FeMn_{10}Ti_{20}$-N catalyst (Fig. 1.3B).

Table 1.1. The composition of the catalysts from XRF results.

Catalysts	Catalysts composition from XRF (wt. %)				Molar ratio of each component
	K	Fe	Mn	Ti	(K/Fe/Mn/Ti)
Fe	-	97.5	-	-	-/90/-/-
K_3/Fe	1.1	96.0	-	-	1.5/90/-/-
$FeMn_{10}$	-	89.1	8.6	-	-/90/8.8/-
$FeTi_{20}$	-	84.4	-	13.8	-/90/-/17.2
$K_3/FeMn_{10}Ti_{20}$	1.2	76.1	7.8	12.8	2.0/90/9.3/17.6
$FeMn_{10}Ti_{20}$	-	76.5	7.7	14.2	-/90/9.2/19.5
$K_1/FeMn_{10}Ti_{20}$	0.4	76.5	7.9	12.8	0.7/90/9.4/17.5
$K_5/FeMn_{10}Ti_{20}$	2.3	76.3	7.8	12.4	3.9/90/9.3/17.1
$K_3/FeTi_{20}$	1.3	84.7	-	12.1	2.0/90/-/15.0
$K_3/FeMn_5Ti_{20}$	1.3	80.4	3.7	12.1	2.1/90/4.2/15.8
$K_3/FeMn_{20}Ti_{20}$	1.2	67.7	15.5	12.9	2.3/90/20.9/20.0
$K_3/FeMn_{10}$	1.4	88.0	9.1	-	2.0/90/9.5/-
$K_3/FeMn_{10}Ti_{10}$	1.3	82.2	8.1	6.2	2.0/90/9.1/7.9
$K_3/FeMn_{10}Ti_{30}$	1.2	69.1	7.0	19.9	2.1/90/9.2/30.2
$K_3/FeMn_{10}Ti_{20}$-N	1.3	74.5	7.5	14.6	2.3/90/9.2/20.6

Table 1.2. Texture properties of TiO_2 and Alk-TiO_2.

Samples	Specific surface area [a] (m^2/g)	Total pore volume [b] (cm^3/g)	Average pore diameter (nm)	Crystalline size [c] (nm)
TiO_2	63.3	0.48	30.0	18.3
Alk-TiO_2	283.7	0.85	11.9	8.3

[a] The specific surface area was determined by BET method.

[b] The total pore volume was determined by BJH method.

[c] The crystalline size was calculated by Scherrer formula.

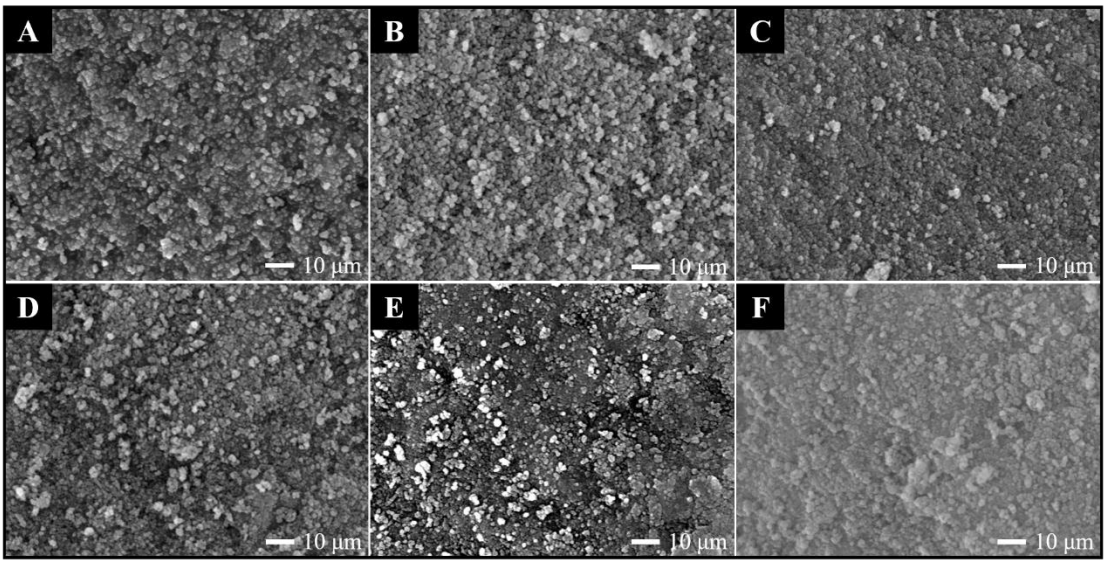

Fig. 1.1. FE-SEM images of Fe (A), K_3/Fe (B), $FeMn_{10}$ (C), $FeTi_{20}$ (D), $K_3/FeMn_{10}Ti_{20}$ (E) and $K_3/FeMn_{10}Ti_{20}$-N (F).

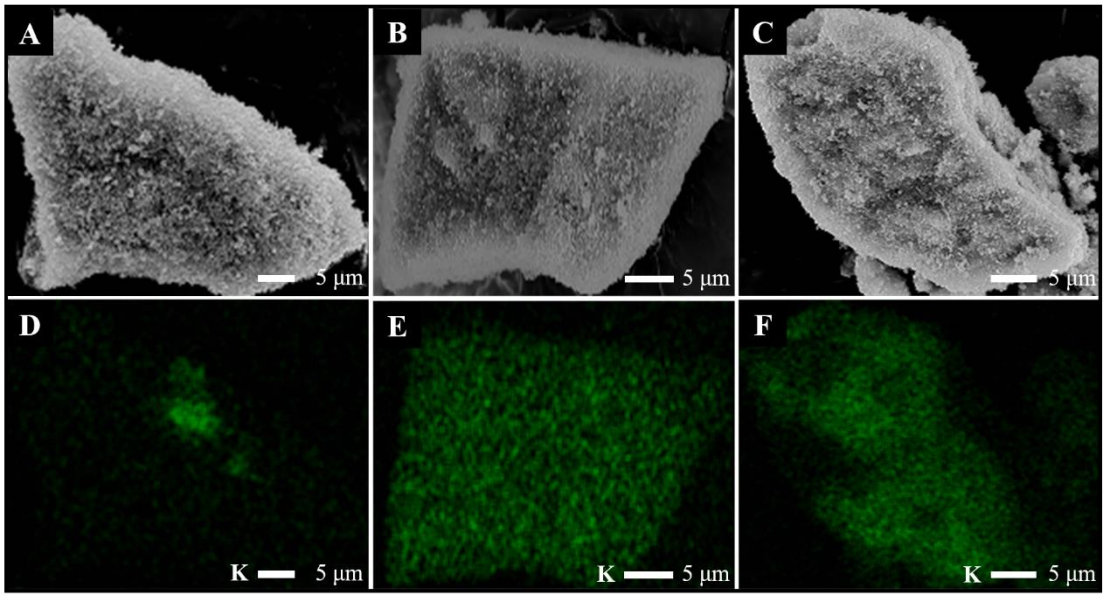

Fig. 1.2. FE-SEM images and EDS mappings of K_3/Fe (A, D), $K_3/FeMn_{10}$ (B, E) and $K_3/FeTi_{20}$ (C, F).

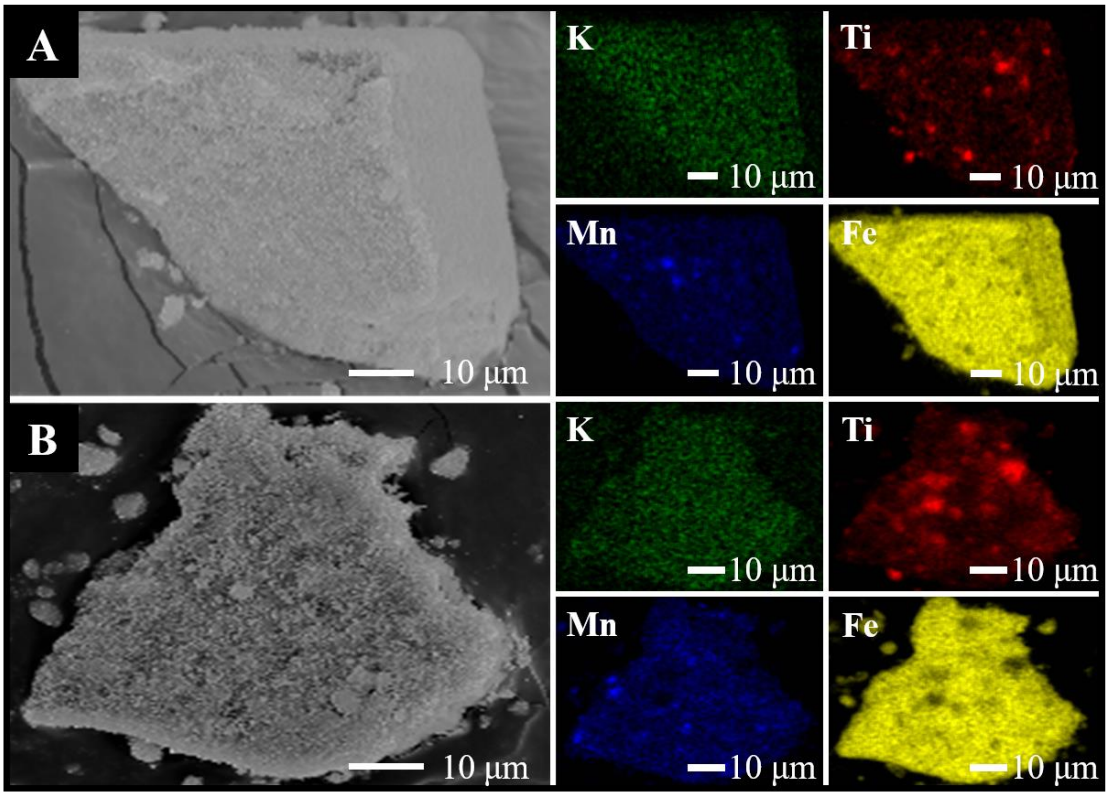

Fig. 1.3. FE-SEM images and EDS mappings of $K_3/FeMn_{10}Ti_{20}$ (A) and $K_3/FeMn_{10}Ti_{20}$-N (B).

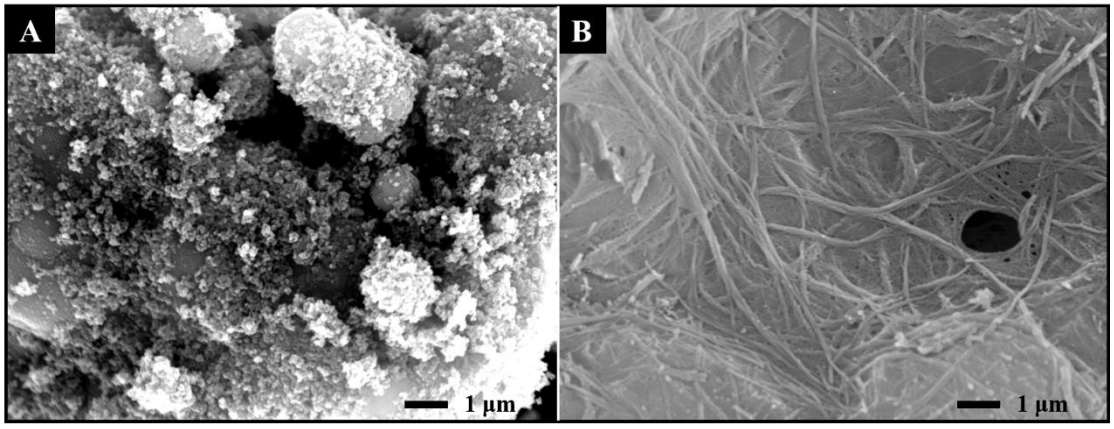

Fig. 1.4. FE-SEM images of TiO_2 (A) and Alk-TiO_2 (B).

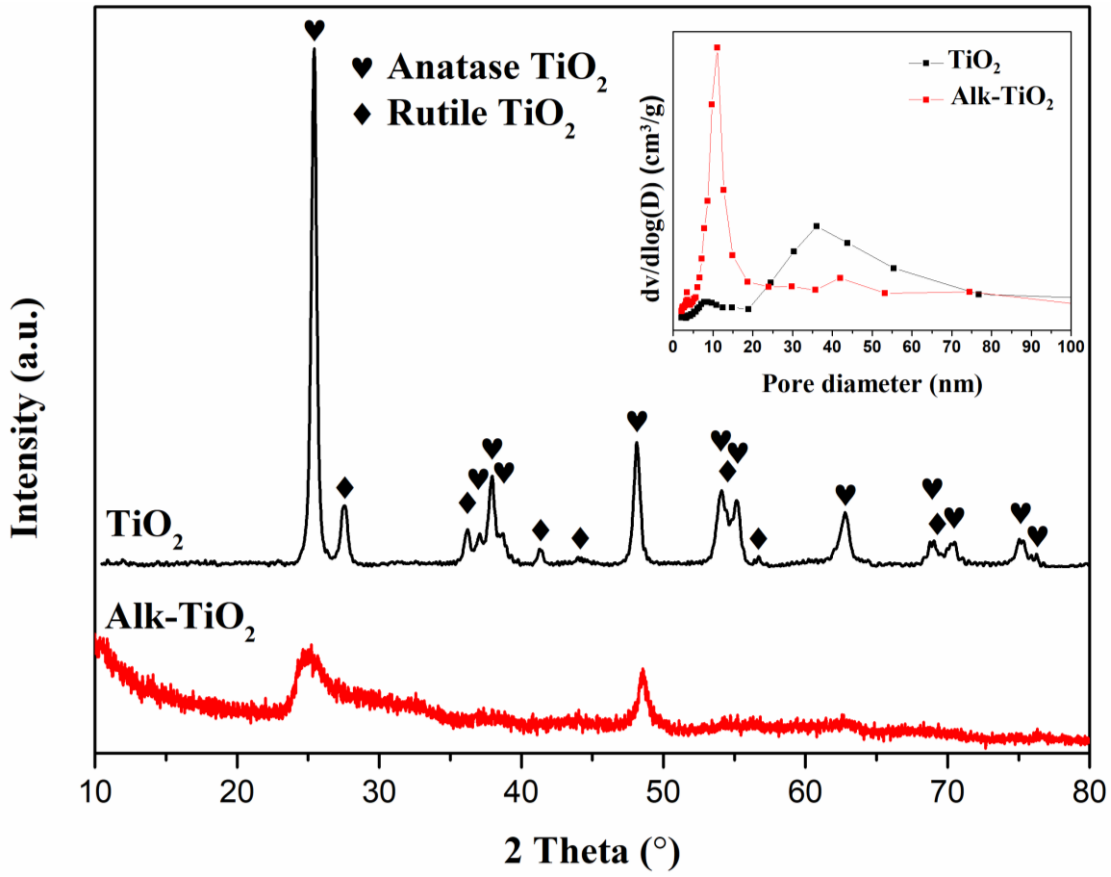

Fig. 1.5. XRD patterns and pore size distributions of TiO_2 and Alk-TiO_2.

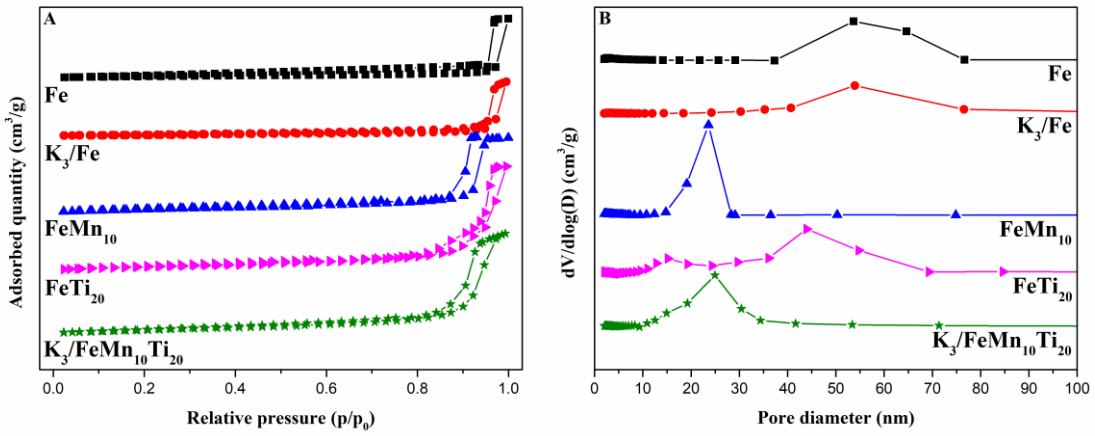

Fig. 1.6. N_2 adsorption-desorption isotherms (A) and pore size distributions (B) of the fresh catalysts with different promoters.

Table 1.3. Texture properties of the fresh catalysts with different promoters.

Catalysts	Specific surface area [a] (m^2/g)	Total pore volume [b] (cm^3/g)	Average pore diameter (nm)	Crystalline size [c] (nm)
Fe	12.2	0.143	47.0	57.7
K_3/Fe	8.5	0.131	61.7	81.2
$FeMn_{10}$	29.8	0.184	24.7	34.5
$FeTi_{20}$	34.1	0.255	29.9	42.4
$K_3/FeMn_{10}Ti_{20}$	41.5	0.248	24.0	28.2

[a] The specific surface area was determined by Brunauer-Emmett-Teller (BET) method.

[b] The total pore volume was determined by Barrett-Joyner-Halenda (BJH) method.

[c] The crystalline size was calculated by Scherrer formula.

Table 1.4. Texture properties of the $FeMn_{10}Ti_{20}$, $K_3/FeTi_{20}$ and $K_3/FeMn_{10}$ catalysts.

Catalysts	Specific surface area [a] (m^2/g)	Total pore volume [b] (cm^3/g)	Average pore diameter (nm)
$FeMn_{10}Ti_{20}$	51.3	0.278	21.7
$K_3/FeTi_{20}$	29.4	0.226	30.8
$K_3/FeMn_{10}$	29.4	0.182	26.3

[a] The specific surface area was determined by Brunauer-Emmett-Teller (BET) method.

[b] The total pore volume was determined by Barrett-Joyner-Halenda (BJH) method.

The texture properties and pore size distributions of the fresh catalysts with various promoters were tested by N_2 adsorption-desorption method, as shown in Fig. 1.6 and Table 1.3. The adsorption-desorption isotherm of type IV was detected for all the catalysts, indicating the existence of mesoporous structure [9]. The pure Fe catalyst exhibited a low specific surface area (12.2 m^2/g) and the pore size mainly centered at 47.0 nm. After the further addition of Mn and Ti, larger specific surface areas were found due to the positive effect of the promoters such as an anti-sintering of iron species with the existence of promoters [17], which could also be proved by the smaller

crystalline sizes (Table 1.3). Meanwhile, the main pore size of $FeMn_{10}$ and $FeTi_{20}$ (about 24.7 nm and 29.9 nm, respectively) became smaller. It should be noticed that a peak centered around 15 nm was found on $FeTi_{20}$ (Fig. 1.6B), which also exited in $FeMn_{10}Ti_{20}$, $K_3/FeTi_{20}$ (Fig. 1.7 and Table 1.4) and $K_3/FeMn_{10}Ti_{20}$. This peak might be considered as being provided by Alk-TiO_2, due to the similar average pore diameter (Table. 1.2). Whereas the existence of K caused a decrease in the specific surface area and an increase in the average pore diameter of the catalysts. As shown in Fig. 1.7, the peaks assigned to the pore smaller than 20 nm became weaker and the pore distributions shifted to higher values at the same time. This phenomenon was consistent with many precious studies reported by others, which attributed to the block of some pores caused by K [22,23]. In addition, the $K_3/FeMn_{10}Ti_{20}$ catalyst exhibited better pore structure because of the joint promoting effect of Mn and Ti. Generally, catalysts with complex pore structure usually cause a relatively long diffusion distance for feeds and products, leading to longer residence time which contributes to the higher selectivity of C_{5+} [24].

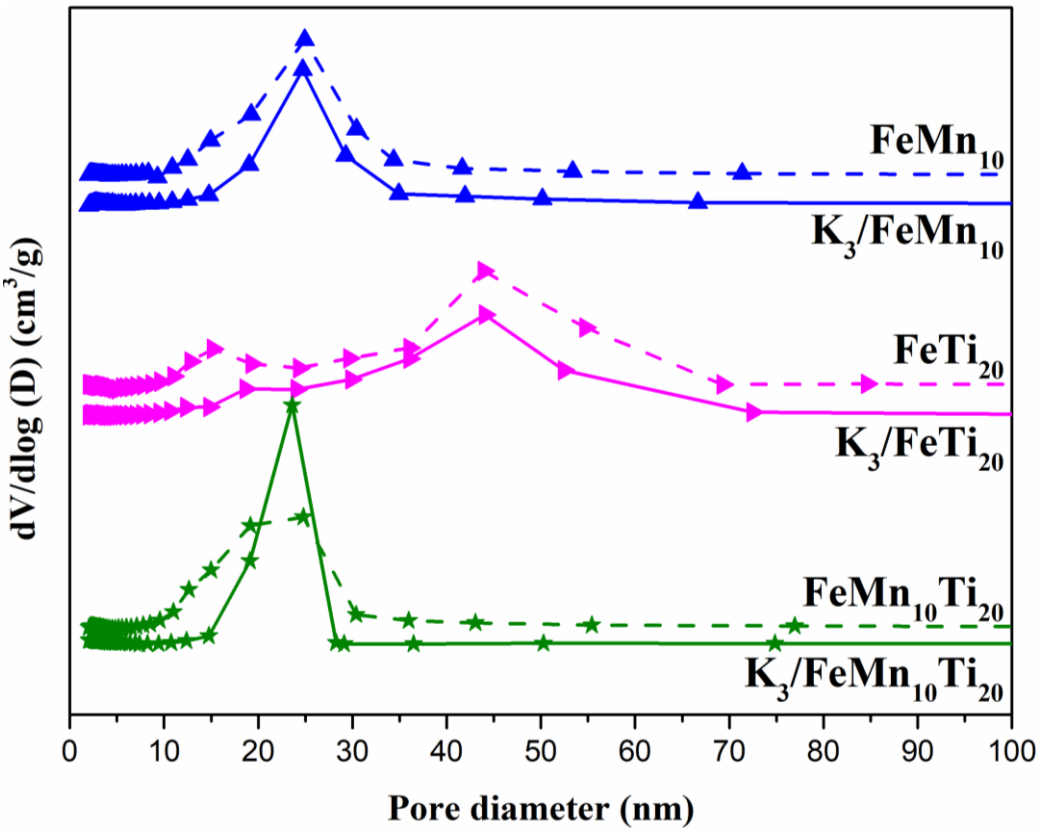

Fig. 1.7. The pore size distributions of the catalysts with or without K.

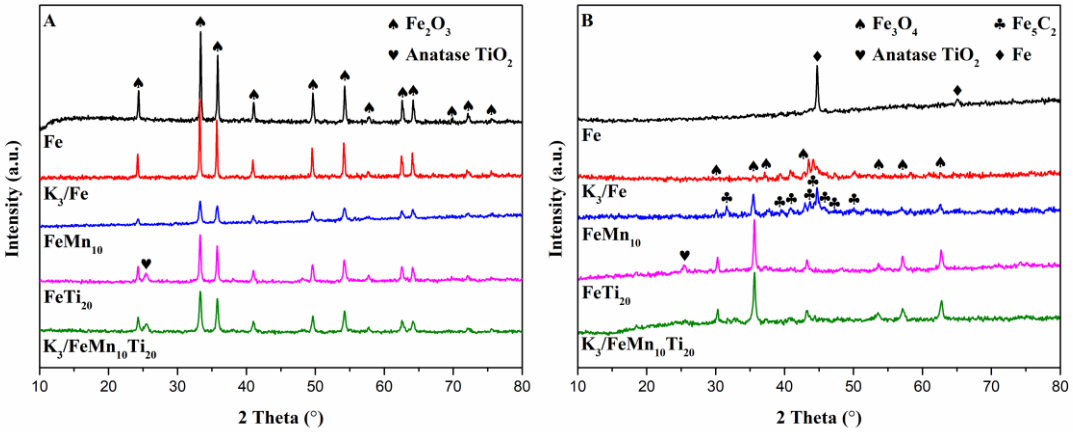

Fig. 1.8. XRD patterns of the fresh (A) and spent (B) catalysts with different promoters.

XRD patterns of the fresh and spent catalysts with different promoters were compared in Fig. 1.8 and the crystalline sizes of fresh catalysts were also shown in Table 1.3. The diffraction peaks assigned to Fe_2O_3 (JCPDS, 33-0664) were detected for all the fresh catalysts [25]. Besides, the diffraction peak at 25.3° was found on the $FeTi_{20}$ and $K_3/FeMn_{10}Ti_{20}$ catalysts, which could be ascribed to the anatase type TiO_2 (JCPDS, 21-1272) [21]. However, no characteristic diffraction peaks associating to K and Mn were detected, suggesting that the potassium oxides and manganese oxides were highly dispersed, which was proved by the results of FE-SEM-EDS. Besides, smaller crystalline sizes were found on $FeMn_{10}$ and $FeTi_{20}$, due to the strong interaction between Fe and Mn or Ti. As a result, the lowest crystallinity and the smallest crystalline size, which are usually considered as signals to better dispersion, were observed on the $K_3/FeMn_{10}Ti_{20}$ catalyst [25]. According to Fig. 1.8B, only the Fe (JCPDS, 06-0696) phase was detected on the spent Fe catalyst, while the diffraction peaks ascribed to Fe_3O_4 (JCPDS, 19-0629) and Fe_5C_2 (JCPDS, 36-1248) were found on other spent catalysts, indicating the addition of promoters were conducive to the carbonization of iron species and the formation of RWGS reaction active sites (Fe_3O_4) [26].

1.3.2 Surface composition properties of different catalysts

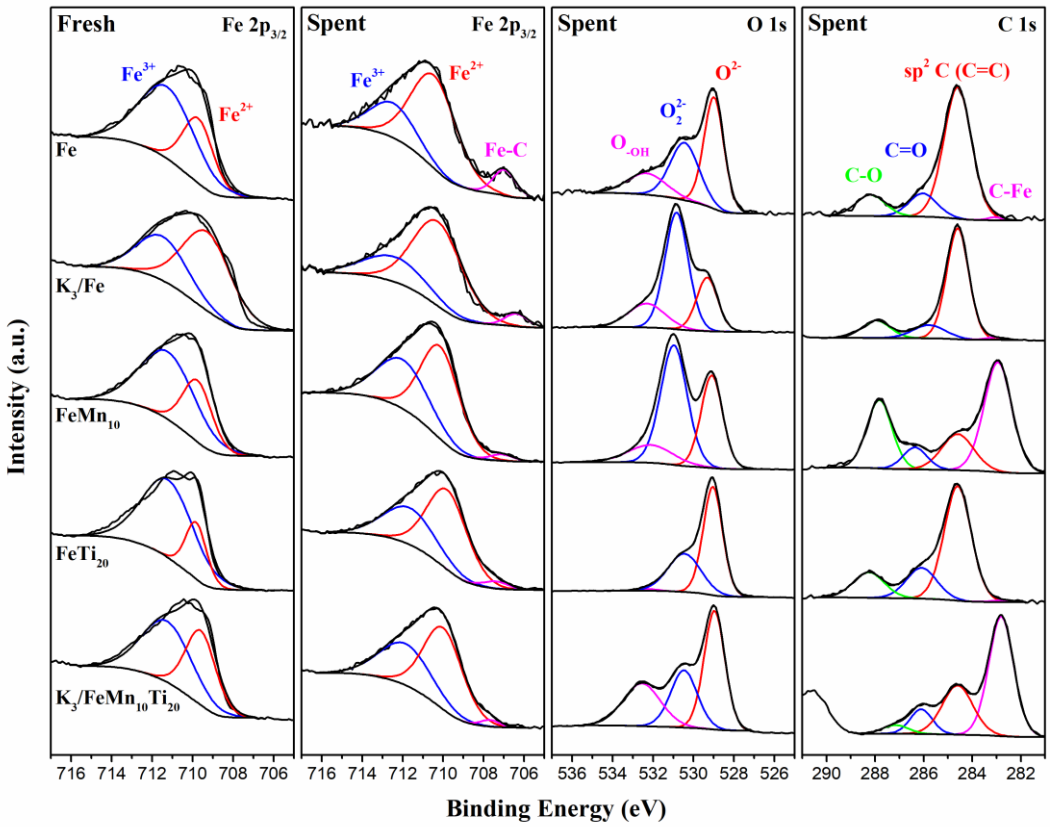

Fig. 1.9. XPS spectra of various fresh and spent catalysts with different promoters.

In order to confirm the surface compositions of various catalysts, XPS characterization was performed and the results were compared in Fig. 1.9 and Table 1.5. Binding energy of Fe $2p_{3/2}$ XPS spectra in the 705-716 eV range was deconvoluted into several peaks which could be assigned to Fe^{3+} (712 eV), Fe^{2+} (710 eV) and Fe-C (707 eV), respectively [27,28]. For C 1s XPS spectra, the peaks around 288 eV, 286 eV, 284.6 eV and 283 eV could be assigned to C-O, C=O, sp^2 C (C=C) and C-Fe, respectively [29,30]. The O 1s XPS spectra could be deconvoluted into three peaks, O^{2-} (529 eV), which could be corresponded to the lattice oxygen species, O_2^{2-} (531 eV) and O_{-OH} (532 eV), which could be both attributed to the surface adsorbed oxygen species [31,32]. Obviously, the introduction of different promoters could regulate the oxygen vacancies as well as adsorption characteristics of the catalysts (Fig. 1.9). Moreover, the

improved surface characteristics including active sites and CO_x adsorption were able to affect the effective match of RWGS and chain propagation.

Table 1.5. The content of Fe^{2+}, Fe-C, $O_{adsorbed}$, C=C and C-Fe on the fresh and spent catalysts with different promoters calculated by XPS.

Catalysts	Fresh (%)	Spent (%)				
	Fe^{2+}/Fe_{total}	Fe^{2+}/Fe_{total}	Fe-C/Fe_{total}	$O_{adsorbed}/O_{total}$	C=C/C_{total}	C-Fe/C_{total}
Fe	33.40	66.18	9.21	52.87	73.23	0.96
K_3/Fe	63.62	69.13	4.89	76.07	71.37	1.45
$FeMn_{10}$	32.70	57.28	2.52	66.13	17.89	47.28
$FeTi_{20}$	22.95	60.68	3.43	37.92	63.59	0.90
$K_3/FeMn_{10}Ti_{20}$	42.64	58.40	2.28	55.81	29.10	56.58

Compared to the results of fresh catalysts, the contents of Fe^{2+} were increased after CO_2 hydrogenation and the peaks assignable to iron carbides were observed (Fig. 1.9 and Table 1.5), indicating that the iron species with high valence were partially transformed into lower-valence states iron species and active carbides during the reaction. According to Table 1.5, when K was introduced, the Fe^{2+} contents of both fresh and spent catalysts were increased, while lesser Fe^{2+} was detected with the addition of other promoters, demonstrating the existence of K was conducive to the formation of active phases (Fe_3O_4) for RWGS reaction. Besides, the highest ratio of $O_{adsorbed}/O_{total}$ was found on K_3/Fe, indicating the existence of abundant oxygen vacancy. Generally, RWGS reaction was based on a redox cycle as follow: Fe^{3+} was first reduced to Fe^{2+} at the H_2 atmosphere and then it would be oxidized by CO_2 with the production of CO. Therefore, the addition of K improved RWGS reaction of catalyst by promoting the reduction of Fe^{3+} to Fe^{2+} and the formation of more oxygen vacancies which facilitated CO_2 adsorption and further reaction [5]. For another reaction (FTS) in the CO_2 hydrogenation, Tsubaki et al. [1] reported that although the content of Fe-C bond

was increased with the addition of Co or Ni, CO_2 hydrogenation over these catalysts led to a high CH_4 selectivity. In the present study, the lower ratios of Fe-C/Fe_{total} were detected with the introduction of the promoters, suggesting that a low CH_4 selectivity would be detected. Meanwhile, C-Fe bond also acts as an important role in the FTS reaction. With the addition of Mn, the catalysts possessed an obviously high concentration of C-Fe bond. Similarly, a catalyst with high concentration of C-Fe bond was found by Guo et al. [33] and reported that the abundant content of C-Fe bond led to a significant improvement in the FTS reaction and olefin yields. It was also proved by Sun et al. [34] that a catalyst possessing more C-Fe bonds could exhibit a high olefin selectivity. Besides, less C=C was found on the $FeMn_{10}$ and $K_3/FeMn_{10}Ti_{20}$ catalysts, indicating that the desorption of carbon species became easy after the introduction of Mn. As a result, more active sites would be exposed. Unfortunately, no positive effect on the surface composition could be seen after the addition of Ti, manifesting as the lower content of active sites on the $FeTi_{20}$ catalyst. Therefore, both RWGS and FTS reactions could be improved over the $K_3/FeMn_{10}Ti_{20}$ catalyst through the joint promoting effect of K and Mn.

1.3.3 Reducibilities and CO_2 adsorption capacities of different catalysts

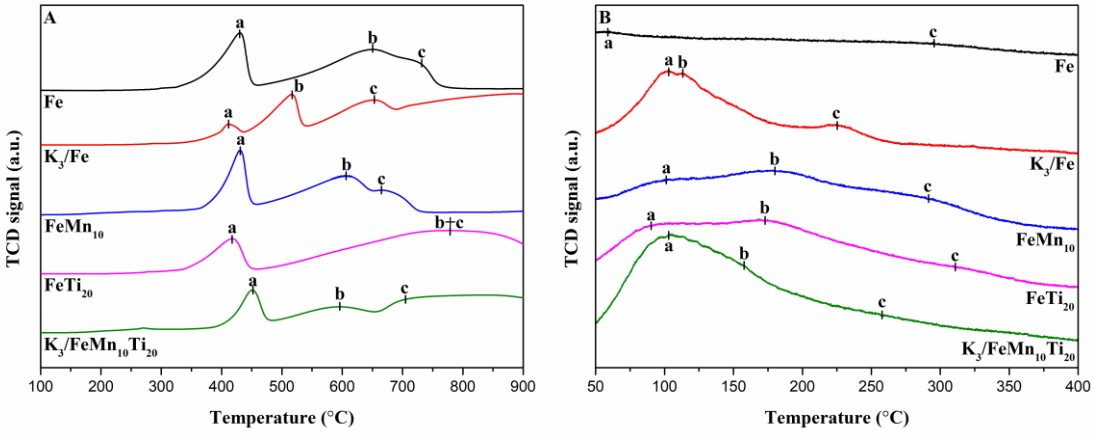

Fig. 1.10. H_2-TPR (A) and CO_2-TPD (B) profiles for the catalysts with different promoters.

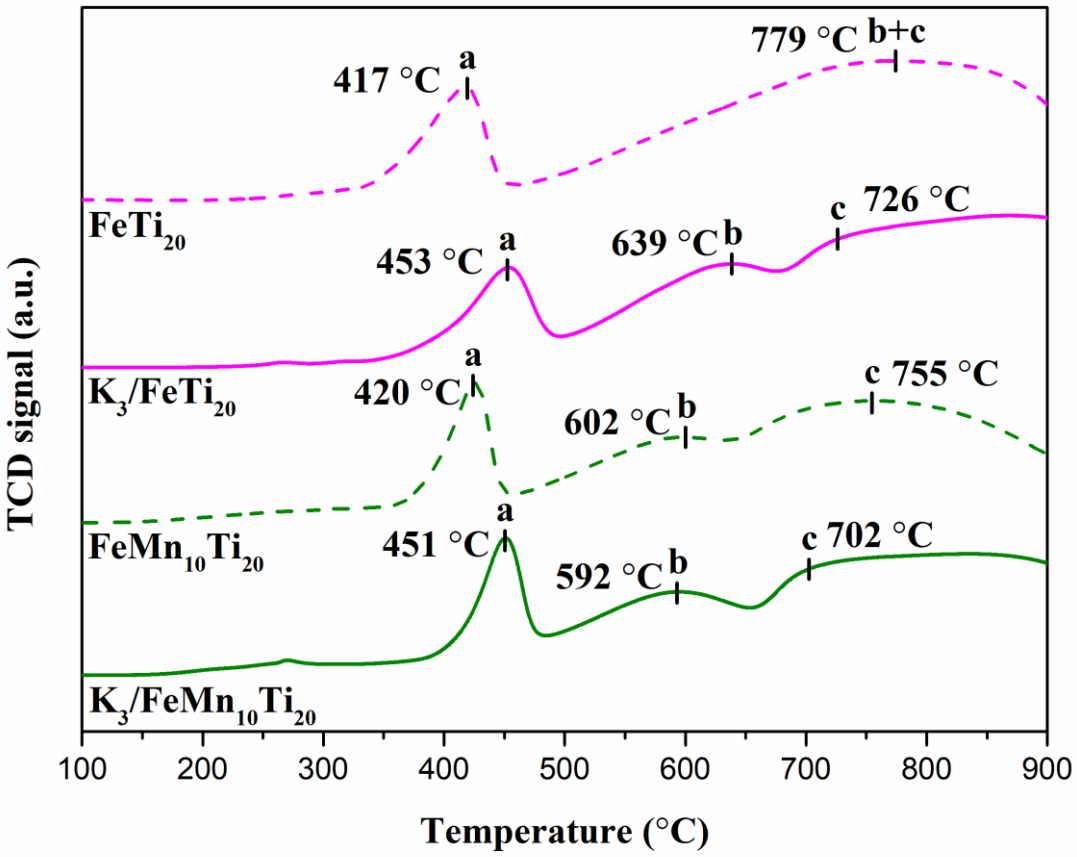

Fig. 1.11. H_2-TPR profiles for the $FeTi_{20}$, $K_3/FeTi_{20}$, $FeMn_{10}Ti_{20}$ and $K_3/FeMn_{10}Ti_{20}$ catalysts.

The reduction behaviors of the catalysts with different promoters were investigated by H_2-TPR and the results were shown in Fig. 1.10A, 1.11 and Table 1.6. Three main reduction peaks were found which could be corresponded to the reduction of Fe_2O_3 to Fe_3O_4 (a), Fe_3O_4 to FeO (b) and FeO to metallic iron (c) [13]. After the introduction of K, the area of peak a was decreased obviously, indicating the lower content of Fe^{3+} over the K_3/Fe catalysts, which was consisted with the results of XPS. Besides, the K_3/Fe catalyst exhibited lower reduction temperature than that of pure Fe catalyst, manifesting the better reducibility. By contrary, no obvious change to the reduction of Fe_2O_3 was found with the addition of Mn. Nevertheless, the reduction temperatures of peak b and c shifted to lower values, indicating the improvement of the reduction behaviors. As for Ti, although the reduction temperature of Fe_2O_3 was

decreased, the reduction of Fe_3O_4 to metallic Fe was suppressed. When K was further incorporated into $FeTi_{20}$, the reduction of Fe_2O_3 was suppressed by regulating the interaction between Fe and Ti, while the promotional effects of K to the reduction of Fe_3O_4 and FeO were not influenced, which could be also proved by those of $FeMn_{10}Ti_{20}$ and $K_3/FeMn_{10}Ti_{20}$ catalysts (Fig. 1.11). Hence, all the three promoters showed positive effects to the reducibilities of the catalysts via different manner, and then higher RWGS reaction activities were realized.

Table 1.6. The reduction temperature, desorption temperature and desorbed amount of CO_2 on the catalysts with different promoters from the results of H_2-TPR and CO_2-TPD.

Catalysts	Reduction Temp. (°C)			Desorption Temp. (°C)			Desorbed amount of CO_2	
	a	b	c	a	b	c	μmol/g	μmol/m^2
Fe	430	650	731	59	-	295	10.1	0.8
K_3/Fe	411	517	653	103	113	225	121.2	14.2
$FeMn_{10}$	430	607	665	101	180	291	141.4	4.7
$FeTi_{20}$	417	779	-	90	173	311	179.2	5.2
$K_3/FeMn_{10}Ti_{20}$	452	595	705	103	158	258	229.8	5.5

As shown in Fig. 1.10B and Table 1.6, the surface basicities of reduced catalysts with different promoters were tested by CO_2-TPD. The desorption peaks lower than 200 °C could be corresponded to the desorption of physical adsorbed (weak) CO_2 on iron (a) and the promoter (b), whereas the peak (c) centered at relatively higher temperature was attributed to the desorption of bridge-bond adsorptive form CO_2 [35]. Among these catalysts, the lowest desorbed amount of CO_2 was detected on the pure Fe catalyst (10.1 μmol/g). With the addition of promoters, K_3/Fe, $FeMn_{10}$ and $FeTi_{20}$ all exhibited more basic sites, and the highest desorbed amount of CO_2 was found on the $K_3/FeMn_{10}Ti_{20}$ catalyst (229.8 μmol/g) due to the synergistic effect of the three promoters. It has been reported that the better CO_2 adsorption capacity generally led to

an enhancement on the catalytic activity in CO_2 hydrogenation [36]. On the other hand, the initial CO_2 desorption temperature of K_3/Fe was lower than that of others, indicating that the CO_2 adsorbed on the K_3/Fe catalyst was more active. Hence, the K_3/Fe catalyst would exhibit higher RWGS activity and higher selectivity of CO. This speculation was verified by the reaction results described below.

1.3.4 Catalytic performances of different catalysts in the CO_2 hydrogenation

1.3.4.1 The effects of different promoters on catalytic performances

The catalytic performances of the iron-based catalysts modified by different promoters in CO_2 hydrogenation were investigated and shown in Table 1.7. It could be observed that pure Fe catalyst exhibited a rather low CO_2 conversion (13.6 %), a high CH_4 selectivity (46.8 %), and small amount of olefin.

Table 1.7. Catalytic performances of the catalysts with different promoters in CO_2 hydrogenation [a].

Catalyst	CO_2 conv. (%)	S_{CO} (%)	Products selectivity (%)				STY of C_{5+} ($g_{fuel}kg_{cat}^{-1}h^{-1}$)	O/P[b]
			CH_4	C_2-C_4	C_{5+}	Oxy		
Fe	13.6	14.2	46.8	36.0	11.4	5.8	46.1	0.22
K_3/Fe	18.4	45.6	16.2	34.1	44.1	5.6	153.8	2.84
$FeMn_{10}$	28.8	4.9	35.0	39.5	20.0	5.5	183.7	0.43
$FeTi_{20}$	24.4	8.4	40.8	39.3	15.5	4.4	116.5	0.30
$K_3/FeMn_{10}Ti_{20}$	34.9	9.7	9.2	27.2	51.0	12.6	556.0	2.68

[a] Reaction conditions: 320 °C, 5.0 MPa, GHSV = 24000 $mLg^{-1}h^{-1}$, $H_2/CO_2/Ar$ = 70.00 v%/25.03 v%/4.97 v%.

[b] O/P means the ratio of olefin (C_{2+}) to paraffin (C_{2+}).

Previously, it had been reported by Khangale et al. [3] and Ying et al. [22] that the competitive adsorption of H_2 and CO_2 occurred on the surface of the catalysts,

indicating that less H_2 could participate in the reaction with the large amount of CO_2 adsorption. As shown in Table 1.6, the K_3/Fe catalyst possessed more basic sites in per unit of specific surface area (14.2 μmol/m^2) than that of other catalysts, resulting in the higher selectivity of C_{5+}, as well as higher yield of olefin. Besides, with the addition of K, more Fe^{2+} and oxygen vacancies were formed and then led to the enhancement of the RWGS reaction, achieving a high CO selectivity (45.6 %). However, the low iron carbides content resulted in the accumulation of CO-intermediates and the improvement of CO_2 conversion was not obvious. Compared to the pure Fe catalyst, although a significant increase of oxygen vacancy was found on the $FeMn_{10}$ catalyst (Table 1.5, O_{ads}/O_{total} from 52.87 % to 66.13 %, C-Fe/C_{total} from 0.96 % to 47.28 %), these abundant FTS reaction active sites, provided by a large amount of C-Fe bond, could lead to the rapid consumption of CO. As a result, the lowest CO selectivity (4.9 %) and higher CO_2 conversion (28.8 %) were detected on $FeMn_{10}$. According to the previous study, the addition of Mn was beneficial to the production of light olefin, which plays an important role for the following chain propagation [37]. Therefore, $FeMn_{10}$ showed higher selectivity of C_{5+} (20.0 %) than that of pure Fe catalyst, which was ascribed to the well dispersion of active sites and the smaller crystalline size. In addition, the better catalytic performance than pure Fe catalyst was observed after the addition of Ti, although fewer active species was detected on $FeTi_{20}$ (Table 1.5). Fortunately, outstanding CO_2 adsorption capacity and smaller pore size resulted from Ti led to the fact that more CO_2 involved in the reaction and the residence time of the reactants was extended. Therefore, both higher CO_2 conversion (24.4 %) and C_{5+} selectivity (15.5 %) were found on the $FeTi_{20}$ catalyst.

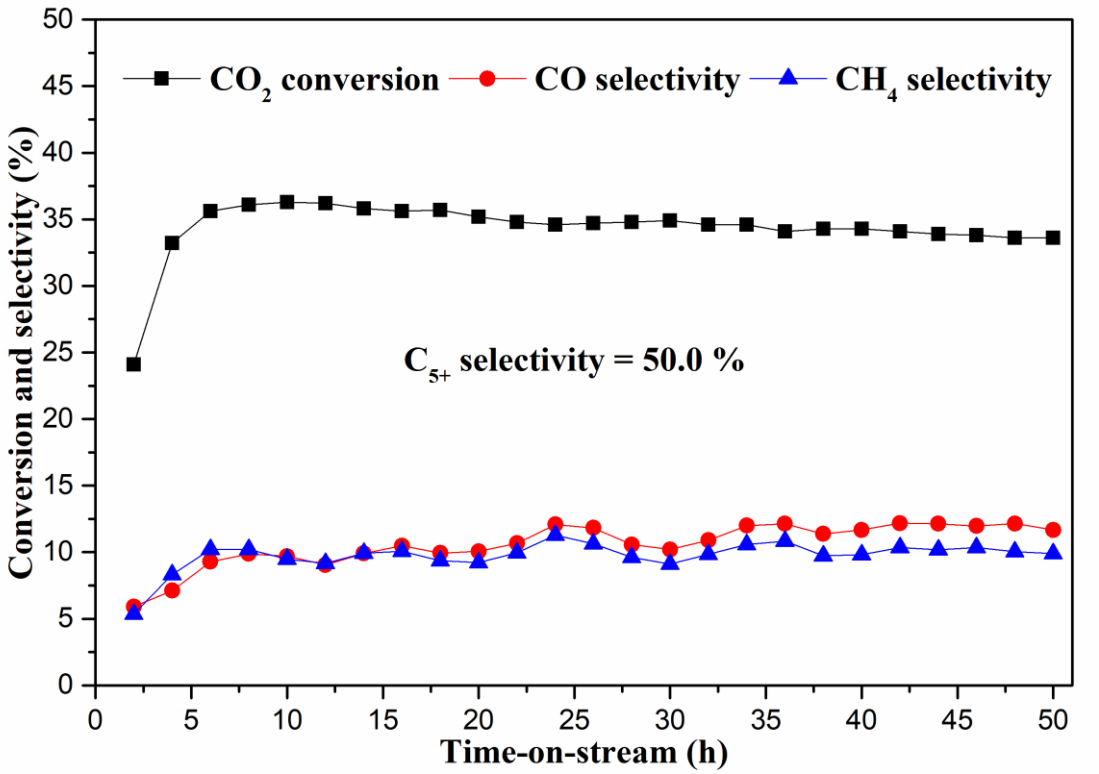

Fig. 1.12. Stability test of the $K_3/FeMn_{10}Ti_{20}$ catalysts in CO_2 hydrogenation under the conditions as follow: 320 °C, 5.0 MPa, GHSV = 24000 $mLg^{-1}h^{-1}$, $H_2/CO_2/Ar$ = 70.00 v%/25.03 v%/4.97 v%.

According to the above discussion, each promoter improved the catalytic performance over the iron-based catalyst via different aspects. During the process of CO_2 hydrogenation, CO_2 was first converted to CO through the RWGS reaction, followed by subsequent hydrogenation of CO to hydrocarbons via FTS. Therefore, the CO_2 conversion and products distributions of the catalyst cannot be optimized simultaneously just by improving only one of these two steps. When K was incorporated alone as an efficient promoter for RWGS, a large amount of CO was accumulated. Similarly, although the addition of Mn increased the content and exposure of FTS-active sites, CO_2 conversion was limited owing to the lower activity of RWGS reaction. As a result, the $K_3/FeMn_{10}$ catalyst exhibited better catalytic performance due to the synergetic effects between K and Mn (Table 1.8). In addition, CO_2 conversion and C_{5+} selectivity were further improved with the incorporation of Ti. More

importantly, the rather low CH_4 selectivity (9.2 %) and ultra-high STY of C_{5+} (556.0 $g_{fuel}kg_{cat}^{-1}h^{-1}$) were achieved over the $K_3/FeMn_{10}Ti_{20}$ catalyst due to the synergistic effects of the multi-promoters, suggesting the well-matching tandem catalysis between the RWGS and chain propagation. Besides, the stability test of the $K_3/FeMn_{10}Ti_{20}$ catalyst was conducted for 50 h and the results were shown in Fig. 1.12. Obviously, CO_2 conversion and products distributions remained stable during the whole period, indicating that the $K_3/FeMn_{10}Ti_{20}$ catalyst could exhibit a well potential industrial application.

Table 1.8. The catalytic performances of the $K_3/FeMn_{10}Ti_{20}$-N catalyst and $K_3/FeMn_{10}Ti_{20}$ catalysts with different contents of each promoter in CO_2 hydrogenation [a].

Catalyst	CO_2 conv. (%)	S_{CO} (%)	Products selectivity (%)				STY of C_{5+} ($g_{fuel}kg_{cat}^{-1}h^{-1}$)	O/P [b]
			CH_4	C_2-C_4	C_{5+}	Oxy		
$K_3/FeMn_{10}Ti_{20}$-N	30.8	13.7	10.7	29.1	43.5	16.7	388.5	3.28
$FeMn_{10}Ti_{20}$	30.4	4.6	31.3	39.5	23.8	5.4	231.3	0.55
$K_1/FeMn_{10}Ti_{20}$	32.9	8.6	15.6	32.7	33.4	18.3	336.8	1.36
$K_5/FeMn_{10}Ti_{20}$	36.2	9.1	9.7	27.8	50.3	12.2	555.5	3.40
$K_3/FeTi_{20}$	32.9	11.8	12.5	34.4	46.9	6.2	456.0	3.76
$K_3/FeMn_5Ti_{20}$	33.9	9.9	10.0	30.5	50.7	8.8	520.2	2.99
$K_3/FeMn_{20}Ti_{20}$	33.3	11.5	10.1	28.6	50.3	11.0	497.1	2.39
$K_3/FeMn_{10}$	29.2	16.9	9.2	27.9	50.1	12.8	408.4	3.05
$K_3/FeMn_{10}Ti_{10}$	32.4	10.9	9.2	26.2	50.1	14.5	486.1	2.60
$K_3/FeMn_{10}Ti_{30}$	31.7	12.1	12.5	32.7	44.7	10.1	418.0	2.90

[a] Reaction conditions: 320 °C, 5.0 MPa, GHSV = 24000 $mLg^{-1}h^{-1}$, $H_2/CO_2/Ar$ = 70.00 v%/25.03 v%/4.97 v%.

[b] O/P means the ratio of olefin (C_{2+}) to paraffin (C_{2+}).

1.3.4.2 The effects of promoter content on catalytic performances

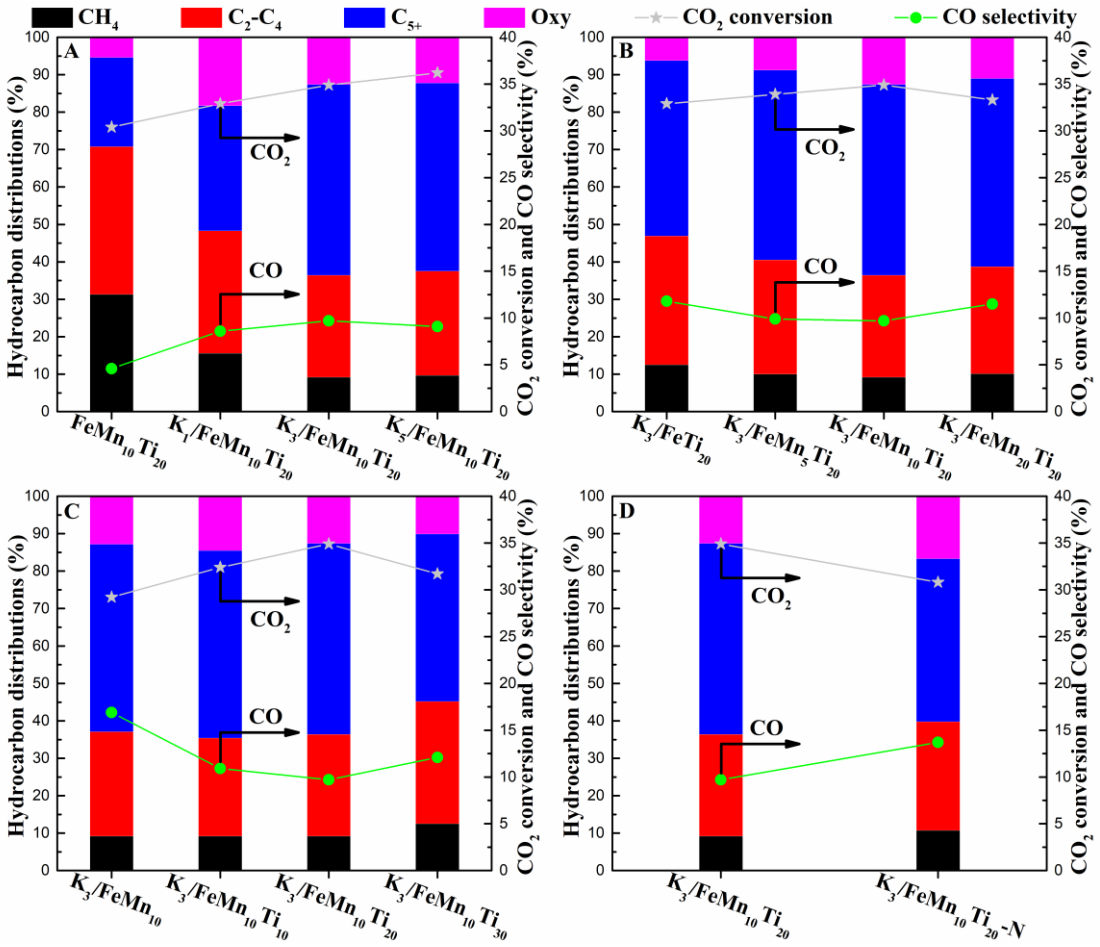

Fig. 1.13. The catalytic performances of the $K_3/FeMn_{10}Ti_{20}$ with different contents of K (A), Mn (B), Ti (C) and the $K_3/FeMn_{10}Ti_{20}$-N catalyst prepared by TiO_2 without pretreatment (D) in CO_2 hydrogenation under the conditions as follow: 320 °C, 5.0 MPa, GHSV = 24000 $mLg^{-1}h^{-1}$, $H_2/CO_2/Ar$ = 70.00 v%/25.03 v%/4.97 v%.

The effects of promoter content in the $K_3/FeMn_{10}Ti_{20}$ catalyst during CO_2 hydrogenation were compared in Fig. 1.13 and Table 1.8. Obviously, $FeMn_{10}Ti_{20}$ showed high CH_4 selectivity (31.3 %) before the introduction of K (Fig. 1.13A). As discussed above, the main effect of K was the improvement of RWGS reaction and the stronger competitive adsorption between CO_2 and H_2. Therefore, more olefin was produced, and higher CO_2 conversion was found with the increase of K content. When the molar ratio of K/Fe was 3/90, the catalyst showed better catalytic performance.

Besides, $K_5/FeMn_{10}Ti_{20}$ (Table 1.8) showed lower CO selectivity and higher CH_4 selectivity than that of $K_3/FeMn_{10}Ti_{20}$ (Table 1.7), which could be explained as the fact that the further increase of K content made the iron ions be stabilized at low oxidation state thus restraining their oxidation by CO_2 and the production of CO, and then led to more CH_4 [5].

As depicted in Table 1.8, the $K_3/FeTi_{20}$ catalyst exhibited a high value of O/P (3.76) due to the strong competitive adsorption and excellent pore structure, which was provided by K and Ti, respectively. With the further incorporation of Mn into $K_3/FeTi_{20}$, although the olefin yield of the catalyst might be increased owing to abundant C-Fe bonds, the secondary reactions from light olefin to long-chain hydrocarbons were apparently promoted at the same time [16]. As a result, higher C_{5+} selectivity and lower value of O/P were observed. Meanwhile, both CO selectivity and CH_4 selectivity were decreased and CO_2 conversion was improved (Fig. 1.13B) over $K_3/FeMn_cTi_{20}$ catalysts with the suitable increase of Mn content. This phenomenon could be ascribed to the improvement of dispersion and chain propagation, and the related catalyst reached the optimal performance with the ratio of 10/90 (Mn/Fe). Undesirably, when excessive Mn was added, the original balance was destroyed, which was also reported by Fierro et al. [9] and Wang et al. [38] that only a small doping amount of Mn strongly promoted the CO_2 hydrogenation and the active sites would be covered by the excessive amorphous Mn oxides, meanwhile, the contact between reactant and active sites would be prevented.

A similar result was found on the $K_3/FeMn_{10}Ti_d$ catalysts. When the content of Ti was 20, the $K_3/FeMn_{10}Ti_{20}$ showed the best performance including CO_2 conversion and hydrocarbon distributions (Fig. 1.13C). Because Ti could only enhance the exposure of active sites and extent the residence time, the total amounts of active sites would be reduced with the further introduction of Ti, resulting in the depravation of the catalytic performance. In addition, the effect of the pretreatment on TiO_2 was additively investigated. As shown in Fig. 1.13D, the $K_3/FeMn_{10}Ti_{20}$-N exhibited worse catalytic

performance due to the poorer dispersion of TiO_2 than Alk-TiO_2, which was proved by the results of FE-SEM.

The existence of each promoter showed various promotional effects on CO_2 catalytic performance. As for this catalyst system applying for CO_2 hydrogenation, the best balance between RWGS and chain propagation was achieved when the molar ratio of K/Fe/Mn/Ti was 3/90/10/20 as in Table 1.7 and 1.8.

Table 1.9. The catalytic performances of the $K_3/FeMn_{10}Ti_{20}$ catalyst under various conditions.

Temperature (°C)	Pressure (MPa)	GHSV ($mLg^{-1}h^{-1}$)	CO_2 conv. (%)	S_{CO} (%)	Products selectivity (%)				STY of C_{5+} ($g_{fuel}kg_{cat}^{-1}h^{-1}$)	O/P [a]
					CH_4	C_2-C_4	C_{5+}	Oxy		
320	5.0	24000	34.9	9.7	9.2	27.2	51.0	12.6	556.0	2.68
320	4.0	24000	31.2	12.0	10.0	28.4	49.4	12.2	455.0	3.48
320	3.0	24000	30.7	14.5	10.4	31.7	47.9	10.0	422.4	4.27
320	2.0	24000	28.4	17.9	11.4	36.4	47.1	5.1	368.9	5.19
300	5.0	24000	27.2	13.2	12.3	33.3	47.9	6.5	379.7	2.51
320	5.0	24000	34.9	9.7	9.2	27.2	51.0	12.6	556.0	2.68
340	5.0	24000	40.4	9.0	10.6	29.1	51.0	9.3	629.1	3.27
360	5.0	24000	46.7	9.7	11.7	27.1	50.6	10.6	716.9	4.05
380	5.0	24000	47.9	10.5	12.5	26.8	40.8	19.9	587.2	4.37
320	5.0	2400	36.9	5.5	6.5	19.2	58.7	15.6	68.7	1.46
320	5.0	6000	36.4	9.6	9.0	24.8	56.2	10.0	159.7	2.61
320	5.0	24000	34.9	9.7	9.2	27.2	51.0	12.6	556.0	2.68
320	5.0	48000	32.7	12.4	10.9	30.5	48.0	10.6	922.7	2.91
320	5.0	120000	24.7	26.6	14.8	38.3	43.8	3.1	1330.8	3.39
360	5.0	48000	44.9	9.6	12.8	30.7	47.0	9.5	1282.7	5.45

[a] O/P means the ratio of olefin (C_{2+}) to paraffin (C_{2+})

1.3.4.3 The effects of reaction conditions on catalytic performances

In order to obtain the best catalytic performance, the $K_3/FeMn_{10}Ti_{20}$ catalyst was tested under various conditions and the results were shown in Fig. 1.14 and Table 1.9. As the reaction pressure decreased from 5.0 MPa to 2.0 MPa, the CO_2 conversion decreased from 34.9 % to 28.4 % (Fig. 1.14A). At the same time, its chain growth capacity was weakened, resulting in the increase of CO selectivity and the decrease of C_{5+} selectivity. The influence of reaction temperature had also been investigated (Fig. 1.14B). About 6 % enhancement of CO_2 conversion and no obvious change of C_{5+} selectivity were noted with the increase of only 20 °C until 360 °C, and an outstanding STY of C_{5+} was found at 360 °C. When the reaction temperature was further increased from 360 °C to 380 °C, a significantly decrease of C_{5+} selectivity (9.8 %) and an inconspicuous increase of CO_2 conversion (1.2 %) were observed. Meanwhile, the effects of space velocity were also studied (Fig. 1.14C). With the increase of space velocity, all the parameters of the catalyst got worse except the STY of C_{5+}. When the space velocity was increased to 120000 $mLg^{-1}h^{-1}$, the resistance time of the reactants was decreased obviously, resulting in the high undesired CO (26.6 %) and CH_4 (14.8 %) selectivity, along with lesser secondary reaction. After the consideration of above three factors, the $K_3/FeMn_{10}Ti_{20}$ was tested at 360 °C and 5.0 MPa with a space velocity of 48000 $mLg^{-1}h^{-1}$ (Table 1.9), achieving a splendid STY of C_{5+} (1282.7 $g_{fuel}kg_{cat}^{-1}h^{-1}$) with relative low selectivity of CO (9.6 %) and CH_4 (12.8 %).

Many means can be tailored for increasing long-chain hydrocarbons selectivity in CO_2 hydrogenation [39]. Compared to various iron-based catalysts in previous studies as listed in Table 1.10, the $K_3/FeMn_{10}Ti_{20}$ catalyst exhibited the highest selectivity of C_{5+} (58.7 %), due to the remarkable chain growth capacity. Besides, significantly low selectivity of CO and CH_4 was found, indicating the well-tuned tandem catalysis between RWGS and chain propagation. As a result, ultra-high STY of C_{5+} (1282.7 $g_{fuel}kg_{cat}^{-1}h^{-1}$) than that of others was achieved.

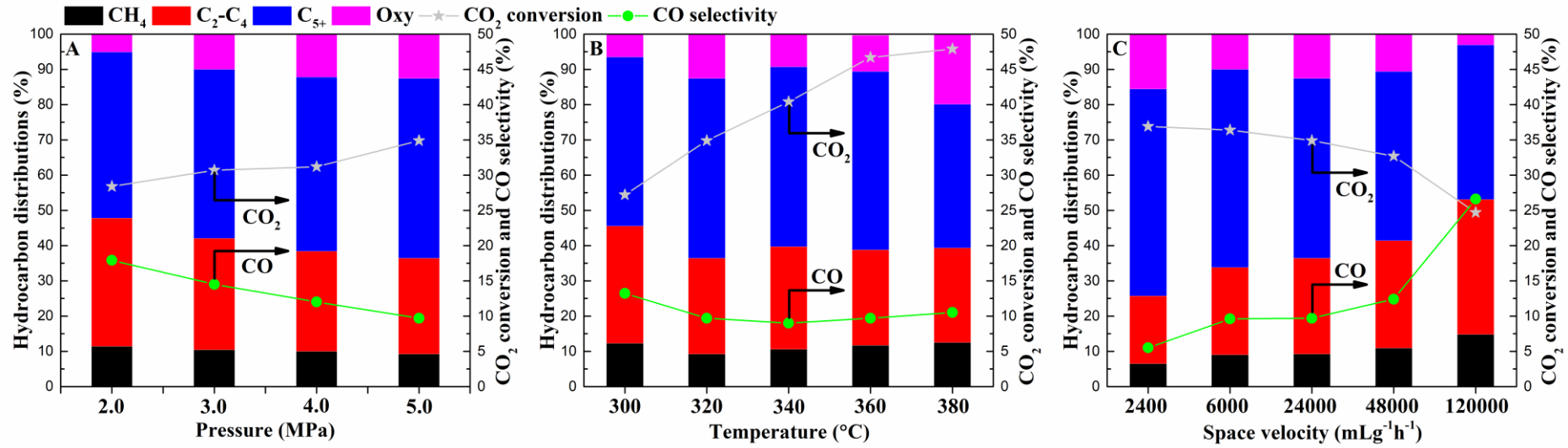

Fig. 1.14. The catalytic performances of the $K_3/FeMn_{10}Ti_{20}$ catalyst under various conditions: pressure (A), temperature (B), space velocity (C) in CO_2 hydrogenation ($H_2/CO_2/Ar$ = 70.00 v%/25.03 v%/4.97 v%).

Table 1.10. Comparison of catalytic performances over various catalysts in CO_2 hydrogenation.

Catalyst	Temperature (°C)	Pressure (MPa)	GHSV ($mLg^{-1}h^{-1}$)	CO_2 conv. (%)	S_{CO} (%)	Hydrocarbon distributions (%)			STY of C_{5+} ($g_{fuel}kg_{cat}^{-1}h^{-1}$)	Reference
						CH_4	C_2-C_4	C_{5+}		
$K_3/FeMn_{10}Ti_{20}$	320	5.0	2400	36.9	5.5	6.5	19.2	58.7	68.7	This study
$K_3/FeMn_{10}Ti_{20}$	360	5.0	48000	44.9	9.6	12.8	30.7	47.0	1282.7	This study
FeMnNa	340	2.0	12000	35.0	18.1	13.1	38.7	48.2	259.1	[13]
FeK/MPC	350	2.5	2000	52.4	5.3	24.4	40.5	35.1	54.4	[25]
$FeAlO_x$-5	330	3.5	4000	36.8	7.2	12.1	30.1	57.8	123.4	[40]
Fe-K/Al_2O_3	300	1.0	2000	27.5	11.6	13.0	36.2	50.8	38.6	[41]
$CuFeO_2$-12	300	1.0	1800	18.1	31.9	3.9	35.8	60.3	20.9	[42]
92.6Fe7.4K	300	2.5	560	41.7	6.0	11.0	29.5	59.5	20.4	[43]

1.4 Conclusion

In summary, iron-based catalysts modified by multi-promoters, including K, Mn and Ti, were prepared by combining co-precipitation method and impregnation method. Compared to pure Fe catalyst, abundant Fe^{2+} and oxygen vacancy, as well as strong competitive adsorption between CO_2 and H_2, were found with the addition of K, contributing to the supervisor RWGS reaction activity and chain growth capacity. However, high chain propagation reaction activity, provided by plentiful C-Fe bonds, was observed with the incorporation of Mn promoter. The introduction of Mn and Ti caused the decrease of crystalline size and promoted the CO_2 adsorption capacity. Meanwhile, Ti provided excellent pore structure, resulting in the long resistance time of CO_2 reactants. Hence, after the optimization of each promoter content, an outstanding promotional tandem catalysis effect on RWGS and chain propagation was achieved with the assistant of the synergistic effect resulted from the three simultaneous promoters above. As a result, the $K_3/FeMn_{10}Ti_{20}$ catalyst possessed low CO and CH_4 selectivity, as well as rather high selectivity of C_{5+}. At the same time, ultra-high STY of C_{5+} than that of other iron-based catalysts was achieved. The results in the present study provided a new insight for the improvement of industrial catalyst via tailoring the balance between RWGS and chain propagation with the help of multi-promoters.

References

[1] L. Guo, J. Li, Y. Zeng, R. Kosol, Y. Cui, N. Kodama, X. Guo, R. Prasert, V. Tharapong, G. Liu, J. Wu, G. Yang, Y. Yoneyama, N. Tsubaki, *Fuel*, 276 (2020) 118102.

[2] J. Li, Y. He, L. Tan, P. Zhang, X. Peng, A. Oruganti, G. Yang, H. Abe, Y. Wang, N. Tsubaki, *Nat. Catal.*, 1 (2018) 787-793.

[3] P.R. Khangale, R. Meijboom, K. Jalama, *J. CO_2 Util.*, 41 (2020) 101268.

[4] J. Wei, J. Sun, Z. Wen, C. Fang, Q. Ge, H. Xu, *Catal. Sci. Technol.*, 6 (2016) 4786-4793.

[5] M. Amoyal, R. Vidruk-Nehemya, M.V. Landau, M. Herskowitz, *J. Catal.*, 348 (2017) 29-39.

[6] N. Boreriboon, X. Jiang, C. Song, P. Prasassrarkich, *J. CO_2 Util.*, 25 (2018) 330-337.

[7] C.G. Visconti, M. Martinelli, L. Falbo, A. Infantes-Molina, L. Lietti, P. Forzatti, G. Iaquaniello, E. Palo, B. Picutti, F. Brignoli, *Appl. Catal. B-Environ.*, 200 (2017) 530-542.

[8] X. An, B. Wu, H. Wan, T. Li, Z. Tao, H. Xiang, Y. Li, *Catal. Commun.*, 8 (2007) 1957-1962.

[9] M. Al-Dossary, A.A. Ismail, J.L.G. Fierro, H. Bouzid, S.A. Al-Sayari, *Appl. Catal. B-Environ.*, 165 (2015) 651-660.

[10] Z. Zhang, C. Wei, L. Jia, Y. Liu, C. Sun, P. Wang, W. Tu, *J. Catal.*, 390 (2020) 12-22.

[11] S. Hwang, S.J. Han, J.E. Min, H. Park, K. Jun, S.K. Kim, *J. CO_2 Util.*, 34 (2019) 522-532.

[12] H. Zhang, H. Zhang, W. Qian, X. Wu, H. Ma, Q. Sun, W. Ying, *Catal. Today*, 388-389 (2022) 199-207.

[13] Y. Xu, P. Zhai, Y. Deng, J. Xie, X. Liu, S. Wang, D. Ma, *Angew. Chem. Int. Ed.*, 132 (2020) 21920-21928.

[14] Q. Chen, W. Qian, H. Zhang, H. Ma, Q. Sun, W. Ying, *Catal. Commun.*, 124 (2019) 92-96.

[15] N. Chaipraditgul, T. Numpilai, C.K. Cheng, N. Siri-Nguan, T. Sornchamni C. Wattanakit, J. Limtrakul, T. Witoon, *Fuel*, 283 (2011) 119248.

[16] L. Falbo, M. Martinelli, C.G. Visconti, L. Lietti, P. Forzatti, C. Bassano, P. Deiana, *Ind. Eng. Chem. Res.*, 56 (2017) 13146-13156.

[17] T. Herranz, S. Rojas, F.J. Pérez-Alonso, M. Ojeda, P. Terreros, J.L.G. Fierro, *Appl. Catal. A-Gen.*, 311 (2006) 66-75.

[18] R.W. Dorner, D.R. Hardy, F.W. Williams, H.D. Willauer, *Catal. Commun.*, 15 (2011) 88-92.

[19] J. Xiao, D. Mao, X. Guo, J. Yu, *Energy Technol.*, 3 (2015) 32-39.

[20] U. Rodemerck, M. Holeňa, E. Wagner, Q. Smejkal, A. Barkschat, M. Baerns, *ChemCatChem*, 5 (2013) 1948-1955.

[21] D.K. Pappas, T. Boningari, P. Boolchand, P.G. Smirniotis, *J. Catal.*, 334 (2016) 1-13.

[22] H. Zhang, H. Ma, H. Zhang, W. Ying, D. Fang, *Catal. Letters*, 142 (2012) 131-137.

[23] H. Wan, B. Wu, C. Zhang, H. Xiang, Y. Li, *J. Mol. Catal. A Chem.*, 283 (2008) 33-42.

[24] X. Wang, D. Wu, J. Zhang, X. Gao, Q. Ma, S. Fan, T.S. Zhao, *Appl. Catal. A-Gen.*, 573 (2019) 32-40.

[25] S.M. Hwang, C. Zhang, S.J. Han, H.G. Park, Y.T. Kim, S. Yang, K.W. Jun, S.K. Kim, *J. CO_2 Util.*, 37 (2020) 65-73.

[26] X. Yang, H. Zhang, Y. Liu, W. Ning, W. Han, H. Liu, C. Huo, *Catalysts*, 9 (2019) 347-360.

[27] S.K. Shaw, S.K. Alla, S.S. Meena, R.K. Mandal, N.K. Prasad, *J. Magn. Magn. Mater.*, 434 (2017) 181-186.

[28] Z. Yang, T. Zhao, X. Huang, X. Chu, T. Tang, Y. Ju, Q. Wang, Y. Hou, S. Gao, *Chem. Sci.*, 8 (2017) 473-481.

[29] S. Wang, T. Wu, J. Lin, Y. Ji, S. Yan, Y. Pei S. Xie, B. Zong, M. Qiao, *ACS Catal.*, 10 (2020) 6389-6401.

[30] S. Jang, S.W. Kang, D.H. Chun, H.T. Lee, J.L. Yang, H. Jung, H.D. Jeong, K.M. Nam, J.C. Park, *New J. Chem.*, 41 (2017) 2756-2763.

[31] Y. Liu, Y. Liu, Y. Guo, J. Xu, X. Xu, X. Fang, J. Liu, W. Chen, H. Arandiyan, X. Wang, *Ind. Eng. Chem. Res.*, 54 (2018) 14052-14063.

[32] X. Zhang, H. Zhao, Z. Song, W. Liu, J. Zhao, Z. Ma, M. Zhao, Y. Xing, *Appl. Surf. Sci.*, 493 (2019) 9-17.

[33] L. Guo, J. Sun, X. Ji, J. Wei, Z. Wen, R. Yao, H. Xu, Q. Ge, *Commun. Chem.*, 1 (2018) 11.

[34] J. Sun, H. Xu, G. Liu, P. Zhu, R. Fan, Y. Yoneyama, N. Tsubaki, *ChemCatChem*, 7 (2015) 1642-1645.

[35] L. Zhang, Y. Zhang, S. Chen, *Appl. Catal. A-Gen.*, 415-416 (2012) 118-123.

[36] T. Wu, J. Lin, Y. Cheng, J. Tian, S. Wang, S. Xie, Y. Pei, S. Yan, M. Qiao, H. Xu, B. Zong, *ACS Appl. Mater. Interfaces*, 10 (2018) 23439-23443.

[37] O.A. Ojelade, S.F. Zaman, *J. CO_2 Util.*, 47 (2021) 101506.

[38] J. Jiang, C. Wen, Z. Tian, Y. Wang, Y. Zhai, L. Chen, Y. Li, Q. Liu, C. Wang, L. Ma, *Ind. Eng. Chem. Res.*, 59 (2020) 2155-2162.

[39] L. Guo, J. Sun, Q. Ge, N. Tsubaki, *J. Mater. Chem. A*, 6 (2018) 23244-23262.

[40] M.K. Khan, P. Butolia, H. Jo, M. Irshad, D. Han, K.W. Nam, J. Kim, *ACS Catal.*, 10 (2020) 10325-10338.

[41] L. Zhang, H. Wang, C. Yang, X. Li, J. Sun, H. Wang, P. Gao, Y. Sun, *Catal. Today*, 356 (2020) 613-621.

[42] Y.H. Choi, Y.J. Jang, H. Park, W.Y. Kim, Y.H. Lee, S.H. Choi, J.S. Lee, *Appl. Catal. B-Environ.*, 202 (2017) 605-610.

[43] S. Geng, F. Jiang, Y. Xu, X. Liu, *ChemCatChem*, 8 (2016) 1303-1307.

Chapter 2

Boosting liquid hydrocarbons selectivity from CO_2 hydrogenation by facilely tailoring surface acid properties of zeolite via a modified Fischer-Tropsch synthesis

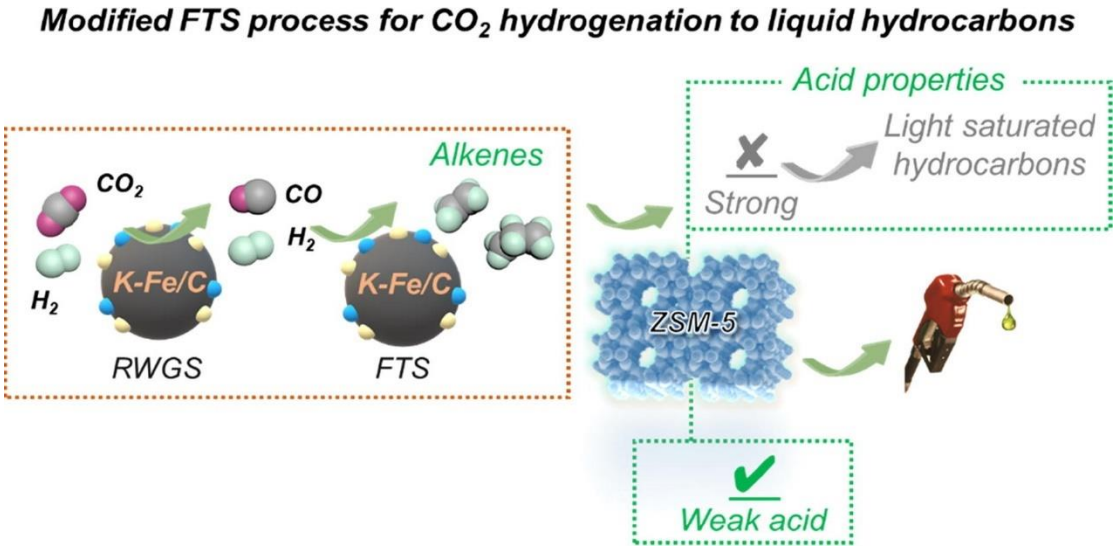

The catalytic performance of CO_2 hydrogenation to liquid fuels over a bifunctional catalyst can be efficiently enhanced via simply tuning the microenvironment properties of ZSM-5 zeolite.

Abstract

Catalytic conversion of greenhouse CO_2 into valuable chemicals or fuels is highly attractive in terms of sustainable development. The chemical inertness of CO_2 molecules and high kinetic barriers for C-C propagation hinder its efficient utilization. In chapter 2, a bifunctional catalyst composed of K-Fe/C and zeolite that efficiently produced liquid fuels via simply tuning the microenvironment properties of ZSM-5 zeolite was reported. The catalysts were characterized by Brunauer-Emmett-Teller (BET), transmission electron microscopy (TEM), X-ray diffractometer (XRD), temperature programmed desorption (NH3-TPD), X-ray photoelectron spectroscopy (XPS). K-Fe/C catalyst was mainly responsible for the formation of olefins, while ZSM-5 catalyst was mainly responsible for olefin secondary reaction, such as aromatization, isomerization, and cracking reaction. Surface acid properties of ZSM-5 could be well regulated through different ion-exchange strategies (such as NH^{4+}, K^+, Na^+, Mg^{2+}, Cu^{2+}, Cs^+, La^{3+}, Ce^{3+} and Mn^{2+}), in which the strong surface acid properties of ZSM-5 were eliminated with the utilization of K^+-ion exchange strategy and then it presented a high C5+ selectivity by suppressing the light saturated hydrocarbons formation. This work provided new insights or facile catalyst treatment for the efficient production of liquid fuels from CO_2 hydrogenation via tuning surface microenvironment properties of ZSM-5 zeolite.

Keyword: CO_2 hydrogenation; Bifunctional catalysts; Zeolites; Heterogeneous catalysis; Ion exchange.

2.1 Introduction

The increasing prominence of environmental problems, such as the global warming, ocean acidification, etc., compels scientists to quest appropriate routes to convert CO_2 into commodity chemicals or fuels [1-5]. The chemical inertness of CO_2 molecules and high kinetic barriers for C–C propagation are two major difficulties in the efficient utilization of CO_2 conversion [6]. Up till present moment, the main catalytic utilization of CO_2, occurring on metallic catalysts or composite catalysts, proceeds via methanol intermediates system or a modified Fischer–Tropsch (F-T) synthesis system [6-8]. As for methanol-mediated process, methanol is first synthesized over methanol catalysts, and then transformed into target products by a series of reactions including dehydration, oligomerization, isomerization, hydrogenation, etc. In the case of a modified F-T process, CO is first generated via reverse water gas shift (RWGS) reaction and then further converted to the target products through chain propagation. Iron-based catalysts are widely used in this process in terms of having two kinds of active sites for RWGS (Fe_3O_4) and chain propagation ability (Fe_xC_y), respectively.

Owing to the convenient transportation, storage and high-density energy, the transformation of CO_2 feedstocks to liquid fuels (C_{5+} hydrocarbons) is a promising means [9-13]. Previously, in order to increase heavy hydrocarbon selectivity, promoters (structural or/and electronic promoters) doping or special structure precursor have been considered [10, 14-17]. Conventional Zn structural promoter and alkaline electronic promoters (especially K and Na) were widely used to improve CO_2 adsorption behavior and active carbide content [14, 18-20]. Electron donating from alkaline promoters to Fe species is beneficial for the formation of electro-rich carbides, presenting a low energy barrier for CO disassociation in addition to stabilize Fe-C bond [18, 21]. Besides, Chio et al. adopted delafossite-$CuFeO_2$ as the catalyst precursor for efficiently converting CO_2 molecules into liquid fuels (C_{5+}) with a high selectivity of 65% [10]. Facile reduction of iron oxide species and selective carburization contribute to the formation

of Hägg iron carbide (Fe_5C_2), which is crucial for the chain propagation behavior [10]. Similarly, a particular spinel-like structure catalyst ($ZnFe_2O_4$) can also achieve an improved heavy hydrocarbon selectivity [14, 19, 22]. It is worth noting that recently He et al. discovered an alloy catalyst (Co_6/MnO_x nanocatalyst) achieving high liquid hydrocarbon selectivity of 53.2% [13]. For this process, CO_2 first adsorbed on the catalyst and was subsequently reduced into CH_2 monomer and CH_3 species, via $CO_2^{\delta-}$, $-CH_2OH$, $HCOO^-$, and/or CH_3O^- intermediates instead of CO intermediates [13].

Considering the ASF distribution limitation that the selectivity of C_{5+} product is less than 53% (α=0.7) [6], bifunctional systems have also been intensively investigated for overcoming this challenge [9, 11]. More recently, composite catalysts have indeed shown excellent catalytic selectivity to produce olefins, aromatics and fuels due to the valid synergetic catalysis among different active sites [9, 11, 23-28]. Gao et al. constructed a bifunctional catalyst composed of partially reduced In_2O_3 and HZSM-5 that could directly convert CO_2 into liquid fuels with an excellent selectivity for value-added products [11]. Thereinto, the oxygen vacancies on the In_2O_3 surface play a crucial role for activating CO_2 to form methanol intermediates [11, 29, 30]. By contrast, Wei et al. designed composite catalysts comprising of Na modified iron catalyst (Na-Fe_3O_4) and zeolite catalysts for selective formation of gasoline-range hydrocarbons or isoparaffins from CO_2 hydrogenation [9, 31]. This multifunctional catalyst possessing three types of active sites (Fe_3O_4, Fe_5C_2 and acid sites), can sequentially cooperatively catalyze CO_2 to CO, CO to alkenes, and alkenes to funded liquid fuels. Clearly, the effective matching manner of different active sites is the prerequisite to achieve this goal [9, 11]. Compared to powder-mixing and dual bed manner, granule-mixing is a suitable proximity to exert benign performance. However, as for a methanol-mediated process over bifunctional systems, one problem that cannot be ignored is the high CO by-product selectivity (generally higher than 45%) [11, 25, 32]. Afterwards, Tan et al. made the target hydrocarbon exhibit a high selectivity, while the selectivity of CO was less than 5% over a In_2O_3/ZrO_2&SAPO hybrid catalyst by optimizing reaction condition [33]. Since zeolite catalysts can directly participate in the catalytic reaction

process, it is obvious that the CO_2 hydrogenation process (i.e. activity and products distribution) can be influenced or regulated by controlling the acidity and pore size of zeolite. Zhang et al. found that the introduction of a small amount of Zn into ZSM-5 by ion-exchange can promote aromatics formation [26]. In addition, the surface acidity of the zeolite can be tailored by coating modification strategy to further improve catalytic performance [23, 32]. Although many efforts have been made for CO_2 hydrogenation, the regulation of zeolite acidity has not received enough attention. The systematic and detailed investigation of zeolite properties is helpful to understand the influence of composite catalyst on the CO_2 hydrogenation process.

Herein, multi-functional catalysts comprising of K-Fe/C and ZSM-5 were adopted for CO_2 hydrogenation to liquid fuels. The microenvironment properties of ZSM-5 were efficiently tuned by treating direct ion-exchange strategy and alkaline solution to adjust surface acid properties and pore size. Through the direct ion-exchange (K^+) of ZSM-5, the catalytic performances over composite catalysts were improved obviously, in which C_{5+} selectivity increased from 39.9% to 70.1% at a CO_2 conversion of 36.2%. For the multi-functional catalysts, ameliorative catalytic performances could be achieved by simply tuning the microenvironment properties of ZSM-5 zeolite, and it provided a new insight for the design of efficient composite catalysts for CO_2 fixation.

2.2 Experiment

2.2.1 Catalyst preparation

Fe/C catalyst was fabricated by hydrothermal synthesis. In brief, 5 g glucose ($C_6H_{12}O_6$) and 6 g iron nitrate ($Fe(NO_3)_3{\cdot}9H_2O$) were dispersed in the deionized water solution. Subsequently, the solution was transformed into a 100 mL capacity Teflon-lined stainless-steel autoclave. It was treated at 150 °C for 24 h to obtain Fe/C catalyst. The detailed processes can also be found elsewhere [20]. The catalytic performance of reference Fe/C catalyst has a lot of room for improvement, thus it is necessary to modify Fe/C catalyst with suitable promoter. K^+ promoter from K_2CO_3 was selected to further

regulate Fe/C. Typically, Fe/C is physically mixed with K_2CO_3 and then was granulated 20 to 40 mesh, marked as K-Fe/C. Thereinto, the loading of K amount equals 6 wt %.

Parent H-ZSM-5 zeolite (Si/Al_2=24) was purchased from Tosoh corporation. Prior to treatment, H-ZSM-5 was calcinated at 550 °C to remove adsorbed water molecules. Afterwards, H-ZSM-5 (1.0g) without alkali solution treatment, was directly treated by one of the nitrate solutions of K^+, Na^+, Cu^{2+}, Mn^{2+}, Mg^{2+}, Ce^{3+}, La^{3+}, or Cs^+ (100 mL, 0.2 mol/L) at 80 °C for 12 h. The filtered zeolites were washed several times with deionized water, and then it was calcined at 550 °C for 5 h. Finally, the obtained products were labelled as X-ZSM-5, in which X stands for the exchanged ion. To further demonstrate the promotional effects, a secondary ion exchange strategy was adopted. Specifically, X-ZSM-5 obtained above was treated with same steps by NH_4^+ solution again to obtain H-ZSM-5*. As for a composite catalyst, it was prepared by simple physical mixing method. For each composite catalyst, Fe-based catalyst of 0.25g (20-40 mesh) was mixed with zeolite of 0.75g (20-40 mesh).

2.2.2 Catalyst characterization

The N_2 physisorption was performed on a NOVA 2200e surface area & pore size analyzer. Prior to texts, the samples were degassed at 200 °C under vacuum conditions for 6 h.

The X-ray diffraction (XRD) spectra were performed on an X-ray diffractometer (Rigaku RINT 2400 X-ray diffractometer) with Cu-Kα radiation (40 kV and 40 mA).

Transmission electron microscopes (TEM) were conducted using a HITACHI H-7650 microscope at an accelerating voltage of 120.0 kV.

X-ray photoelectron spectroscopy (XPS) analysis was conducted on a Thermo Fisher Scientific ESCALAB 250Xi multifunctional X-ray photoelectron spectroscopy instrument.

The acidic properties (NH_3-TPD) of the as-prepared catalysts were measured by using a BELCAT-II-T-SP characterization apparatus. A certain amount of sample (ca. 50 mg) was first reduced at 400 °C in H_2 gas flow (30 mL/min) for 2 h. After reduction,

the temperature of the solid was decreased to 50 °C in He gas flow (30 mL/min). 10 vol % NH_3/Ar gas mixture was then introduced into the reactor for 1 h. Then He was introduced into the reactor to remove gas phase NH_3. The NH_3-TPD trace was recorded from 50 to 900 °C with a heating rate of 10 °C /min.

2.2.3 Catalyst activity evaluation

CO_2 hydrogenation process was evaluated in a fixed-bed reactor with an inner diameter of 6 mm. As-prepared composite catalyst of 1.0 g was in situ reduced at 400 °C for 10 h using pure H_2 flow (40 mL/min, atmospheric pressure). When the temperature dropped to 320 °C, the reactant gas mixture CO_2/H_2/Ar (27.10 v%, H_2: 67.58 v%, Ar: 5.32 v%) was fed into the reactor. At the same time, the pressure rose to 2.0 MPa. CO_2 conversion and CO selectivity were analyzed by an online gas chromatograph (GC) using a thermal conductivity detector (TCD, GC Science 320). The light hydrocarbons were analyzed by an online GC with a flame ionization detector (FID, GC Science 390B). N-octane (C_8) as solvent was equipped to capture the heavy hydrocarbons in the effluents, and the products were analyzed by an off-line GC using an FID. CO_2 conv., S_{CO} and C_i sel. were calculated by the same methods with chapter 1.

2.3 Results

2.3.1 Chemical state of K-Fe/C catalyst

Generally, the phase composition of iron-based catalyst plays critical roles for catalyzing CO_2 hydrogenation. Thus, to reveal the nature of reaction process, K-Fe/C catalyst was studied in detail. As shown in Fig. 2.1, spent K-Fe/C contained nanosized Fe species with an average size of 25 nm. As depicted in high resolution transmission electron microscopy (HR-TEM), two kinds of iron species were detected namely Fe_3O_4 and Fe_5C_2. Fe_3O_4, as a highly active phase for RWGS reaction [9], promotes the CO_2 molecules into CO intermediates. The existence of Fe_5C_2 as crucial active phase makes the chain propagation to form hydrocarbons [9, 20]. Meanwhile, the rate-limiting step of CO_2 hydrogenation over a Fe-based catalyst is the chain growth. In addition, chain

growth, to some extent, can pull the RWGS reaction. On the contrary, a high content of Fe_3O_4 species is not conducive to CO_2 conversion and high hydrocarbon selectivity. Thus, a moderately high ratio of Fe_5C_2 to Fe_3O_4 helps to increase the selectivity of C_{5+} productivity. X-ray photoelectron spectroscopy (XPS) was also applied to investigate the phase composition. As previously reported, the binding energies located at around 711.4, 710.3, and 708.5 eV in the Fe2p spectrum are corresponding to Fe^{III}, Fe^{II}, and Fe-C [20]. Clearly, with the introduction of reaction gas, Fe-C bonds are formed, which are of importance for C-C coupling. Besides, X-ray diffraction (XRD) measurements of as-prepared and spent catalyst are depicted in Fig. 2.1c. As for the as-prepared catalyst, the main phase is humboldtine ($FeC_2O_4 \cdot 2H_2O$ species, JCPDS 23-0293), which is similar to our previous report [34, 35]. After reaction, humboldtine precursor is converted into two main iron species (Fe_3O_4 and Fe_5C_2), which is according to the results of HR-TEM. K promoter is not detected owing to the low content or well dispersion. The utilization of K promoter generally promotes carbide formation for improving chain propagation ability. Meanwhile, the existence of K promoter also suppresses secondary hydrogenation of primary olefins [20], which is beneficial for the formation of alkenes.

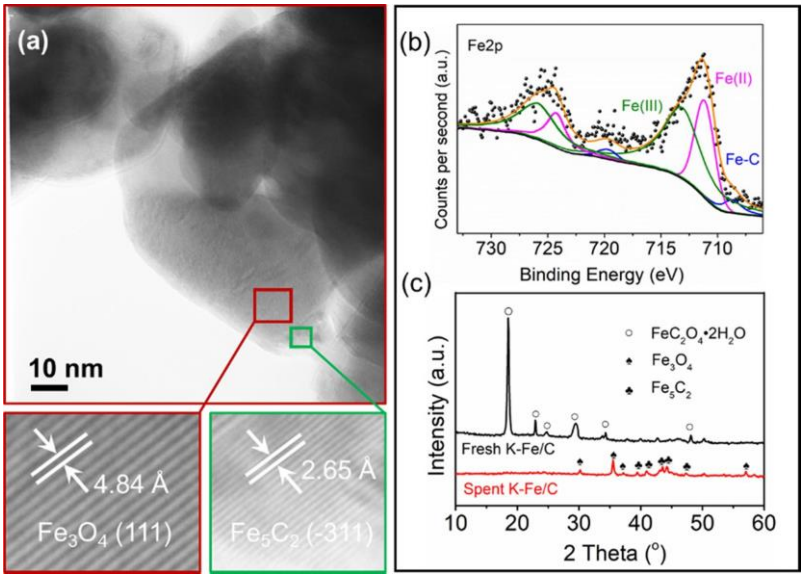

Fig. 2.1. (a) HR-TEM images and (b) Fe2p XPS spectra of spent K-Fe/C; (c) XRD patterns of as-prepared and spent K-Fe/C.

2.3.2 Tunable surface acid properties of ZSM-5 catalyst

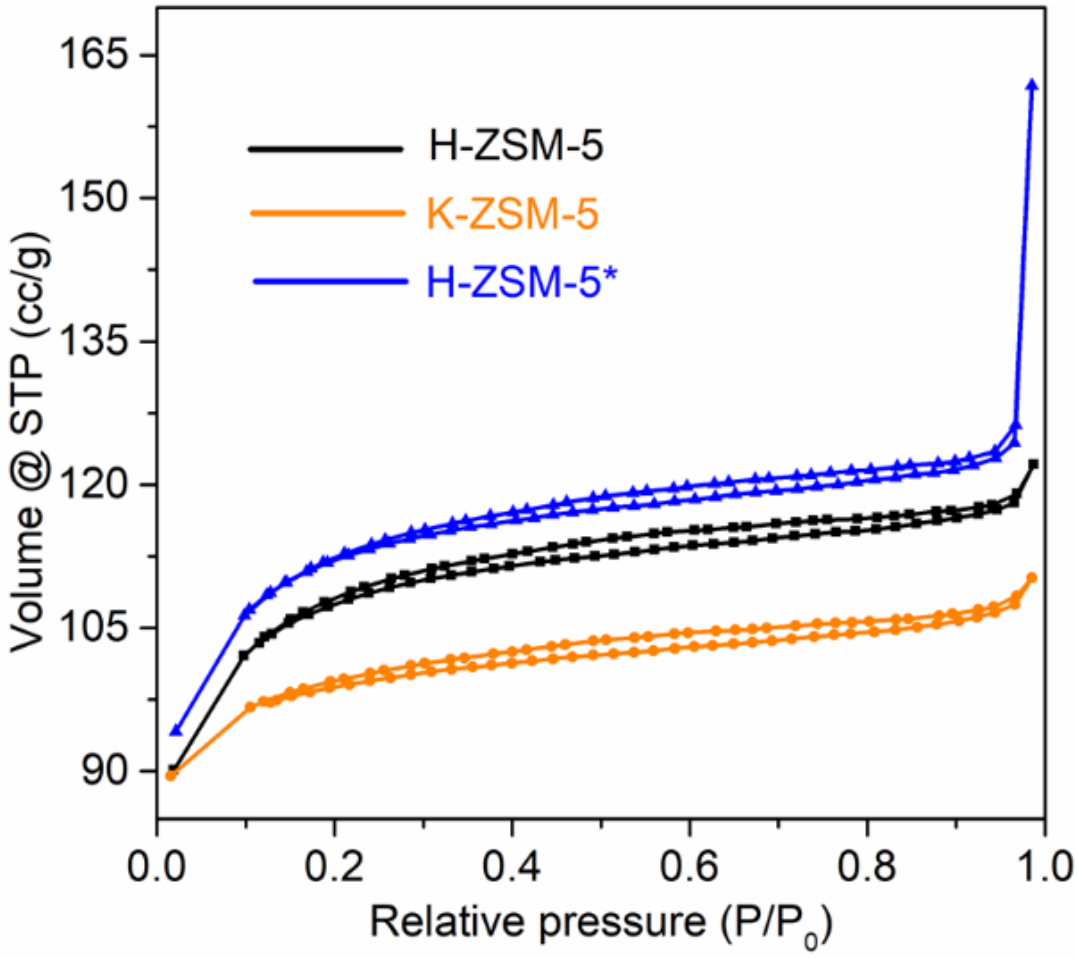

Fig. 2.2. BET and pore size distribution of parent H-ZSM-5, K-ZSM-5, H-ZSM-5*.

Table 2.1. Textural properties of zeolites with different treatments.

Sample	A_{BET}[a] (m^2/g)	A_{ext}[b] (m^2/g)	A_{micro}[b] (m^2/g)	V_{meso}[c] (cm^3/g)	V_{micro}[d] (cm^3/g)
H-ZSM-5	307	15	292	0.02	0.16
K-ZSM-5	276	12	264	0.02	0.15
H-ZSM-5*	322	23	299	0.08	0.17

[a] Surface area evaluated *BET* method.

[b] Surface area evaluated by the *t-pot* method.

[c] Mesopore volume evaluated by the BJH method.

[d] Micropore volume evaluated by the HK method

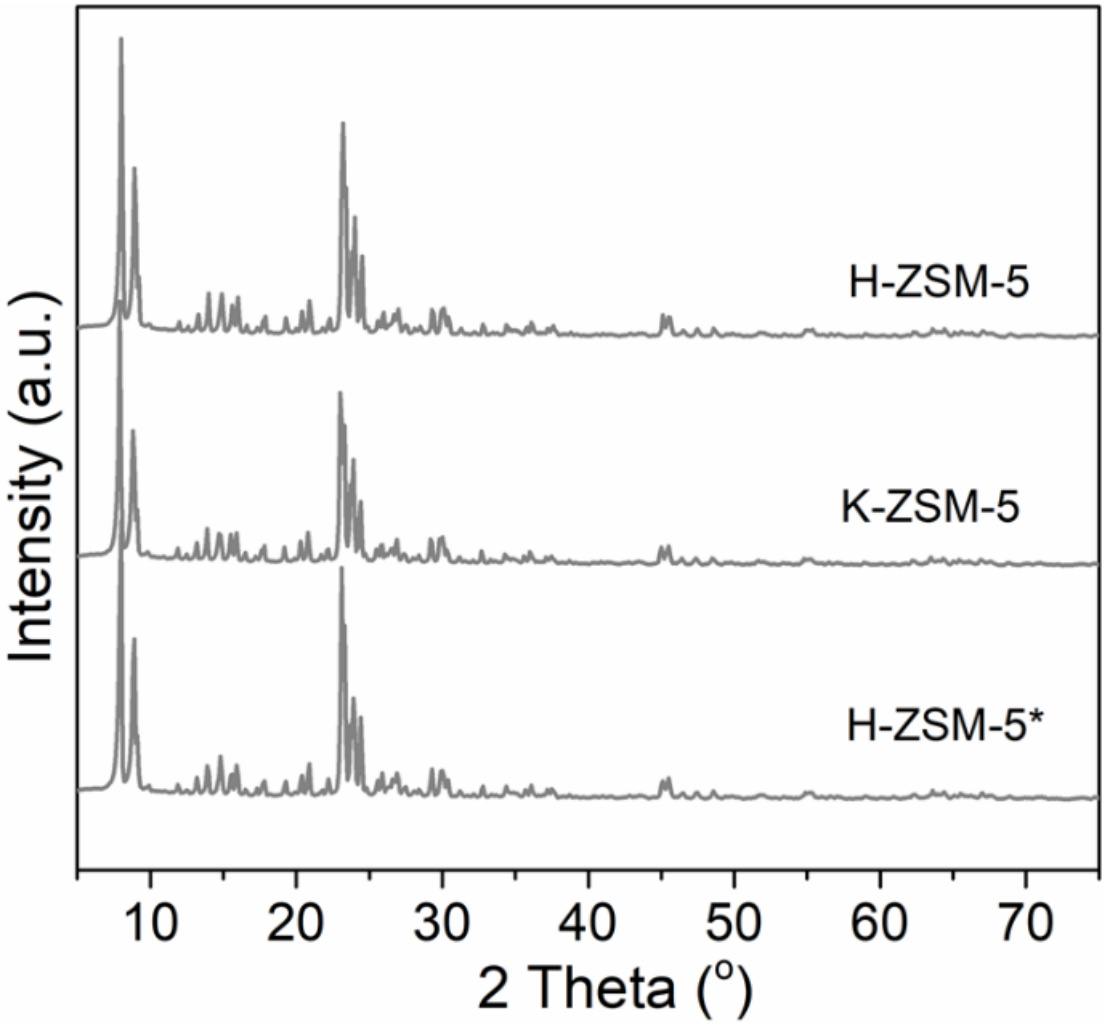

Fig. 2.3. XRD patterns of parent H-ZSM-5, K-ZSM-5, H-ZSM-5*.

The surface acid properties of ZSM-5 zeolite are crucial factors for regulating catalytic performance. Thus, the N_2 adsorption/desorption isotherms of zeolites after various ion treatments were first measured at 77K. According to Fig. 2.2 and Table 2.1, the surface area as well as pore structure of zeolite with various ion treatments changed slightly, indicating that the density change of acid sites on zeolite surface was only related to the acid content. XRD patterns also indicated that different zeolites presented a benign crystal structure (Fig. 2.3). And on this basis, NH_3-TPD profiles for H-ZSM-5, K-ZSM-5, and H-ZSM-5* zeolites were depicted in Fig. 2.4. As seen, there were two distinct desorption peaks of NH_3, one of which desorption peaks of NH_3 at temperature higher than 300 ℃ could be corresponded to the strong interaction between NH_3

molecules and acid sites, and another one at temperature lower 300 °C could be attributed to the weak interaction or/and physical NH_3 adsorption [36-38]. Visibly, different ion exchange strategies significantly changed the acid content of zeolite. As for a typical H-ZSM-5 zeolite, two distinct desorption peaks existed. However, for ZSM-5 zeolite with K^+-ion exchange, characteristic desorption peak at temperature higher than 300 °C almost disappeared, indicating that no strong acid sites existed in K-ZSM-5. When K-ZSM-5 was treated by NH_4^+ to recover H-type ZSM-5, the desorption peak after 300 °C appeared again, indicating that the ion type was closely related to the surface acidity.

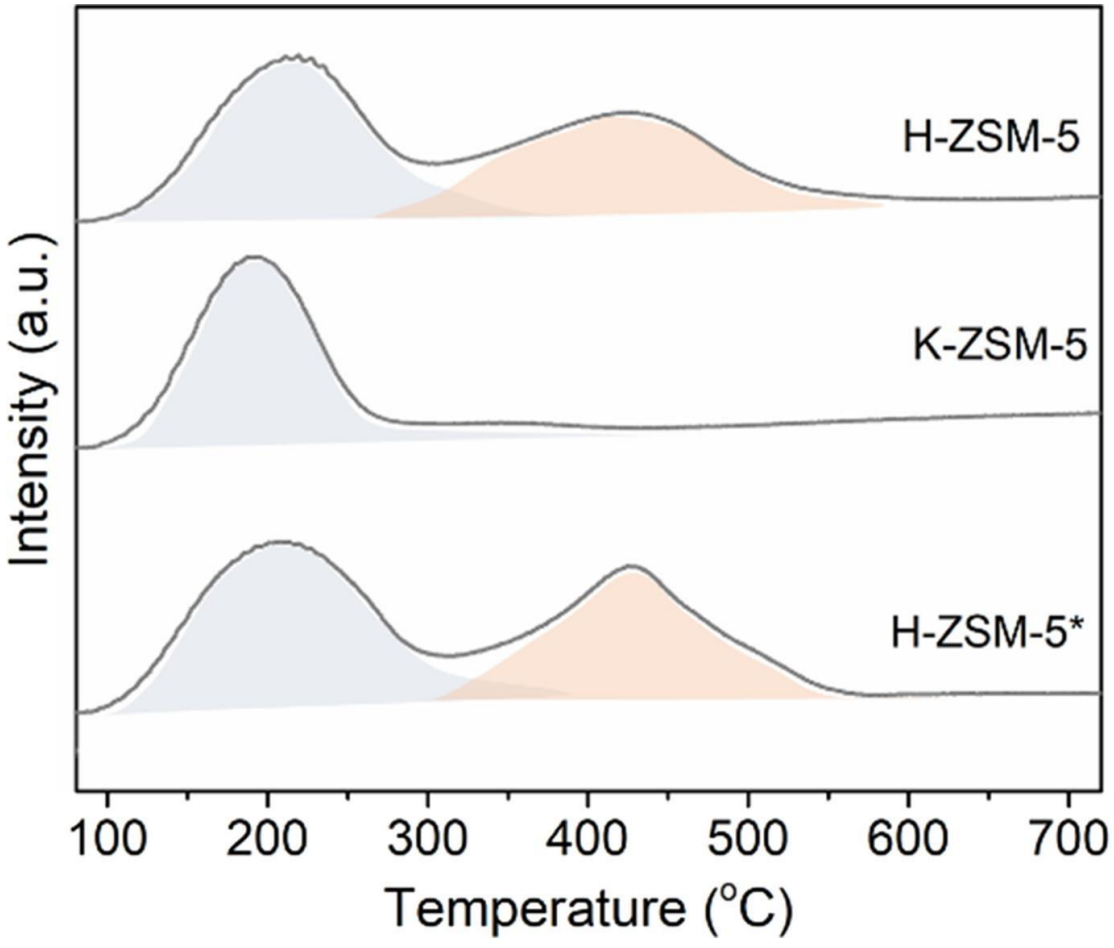

Fig. 2.4. NH_3-TPD profiles of as-prepared H-ZSM-5, K-ZSM-5, and H-ZSM-5* zeolite. H-ZSM-5* represents the H-type ZSM-5 obtained by the first exchange of K^+ and then the exchange of NH_4^+ again.

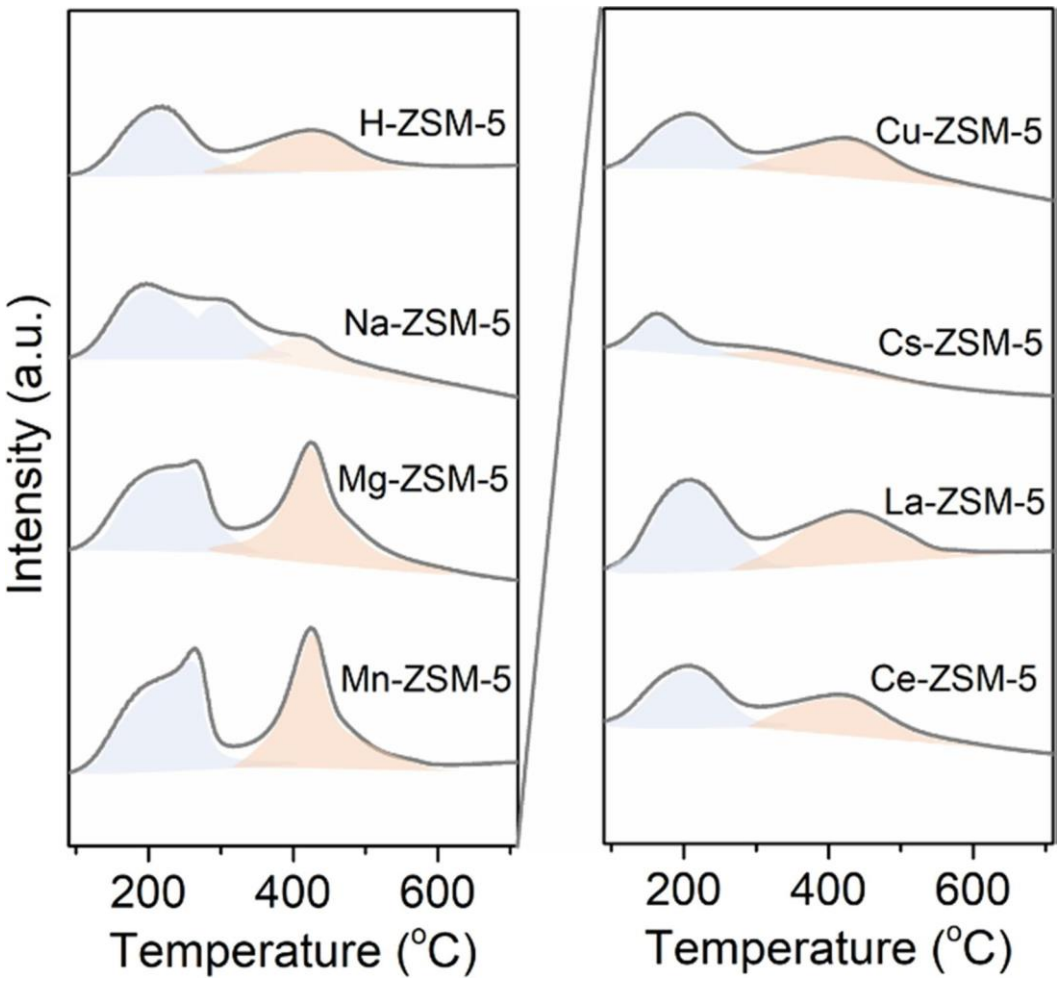

Fig. 2.5. NH_3-TPD profiles of different zeolites with varied ion-exchange strategies.

Table 2.2. The ratio of weak acid to strong acid determined by NH_3-TPD results.

Catalysts	The ratio of weak acid to strong acid
H-ZSM-5	1.1
K-ZSM-5	>100.0
Na-ZSM-5	4.2
Mg-ZSM-5	1.3
Mn-ZSM-5	1.2
Cu-ZSM-5	1.2
Cs-ZSM-5	1.1
La-ZSM-5	1.3
Ce-ZSM-5	1.1

In order to further reveal the effects of direct metal ion exchange strategy on the surface acid properties of ZSM-5, different metal ions (La^{3+}, Na^{+}, Cu^{2+}, Mn^{2+}, Mg^{2+}, Ce^{3+}, and Cs^{+}) were adopted. As drawn in Fig. 2.5, the surface acidity of ZSM-5 changed obviously after different ion exchange treatments. In terms of Na^{+}-ion exchange treatment, the strong surface acid of ZSM-5 (above 300 °C) was decreased, but not as significantly as that of K-ZSM-5. By contrary, the desorption peak intensities of ZSM-5 zeolite treated by Cs^{+}-ion solution decreased obviously in addition to exhibiting the same acidic desorption range. Similarly, unlike the other catalysts, the crystal diffraction intensity of Cs-ZSM-5 is also reduced (Fig. 2.6). Meanwhile, the ratios of weak acid to strong acid of ZSM-5 were summarized in Table 2.2. As compared, strong acid can be visibly eliminated with the treatment of K^{+} or Na^{+} ion, especially K^{+}. On the rest of the metal ions, the ratio between the strong and weak acids did not change significantly. Obviously, the acid content of ZSM-5 can be well regulated by different ion-exchange strategies.

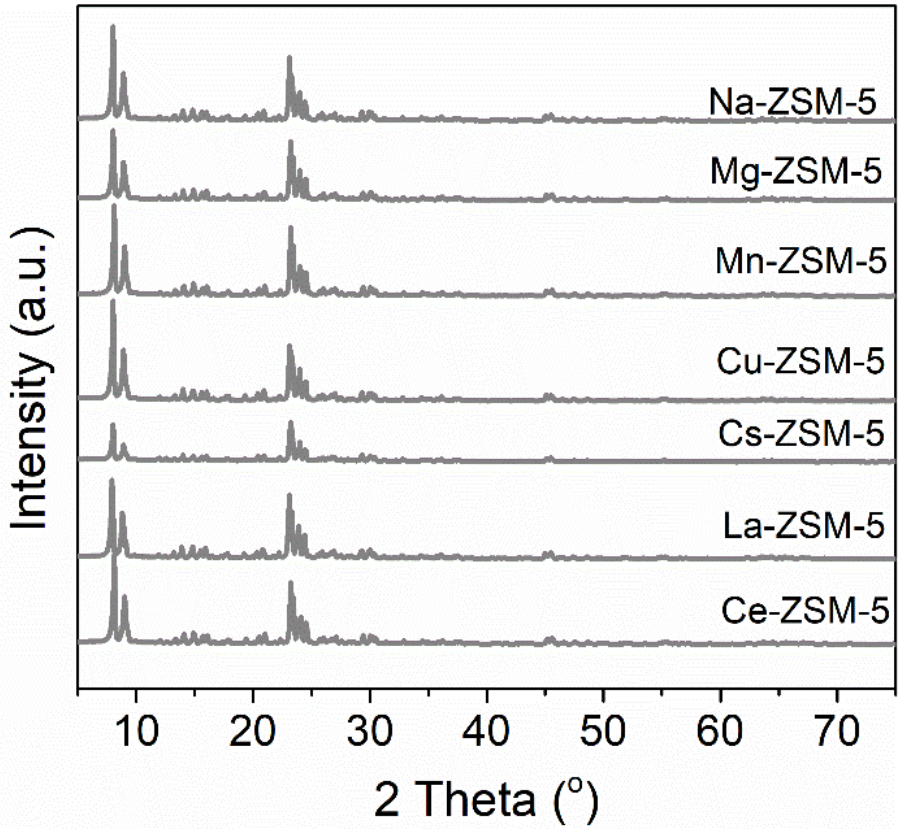

Fig. 2.6 XRD patterns of different zeolites with varied ion-exchange treatments.

2.3.3 Impacts of surface acid microenvironment of ZSM-5 catalyst

Catalytic performance is presented in Fig. 2.7. As seen, K-Fe/C catalyst exhibited a typical ASF distribution, in which CH_4 selectivity was 15.3%, C_2-C_4 selectivity was 43.9%, and C_{5+} selectivity was 40.7% at CO_2 conversion of 35.6% (Table 2.3 and Figure 2.8). Meanwhile, main products were olefins, indicating that K modified Fe/C catalyst exhibited a benign selectivity for olefins formation. In particular, CO_2 molecules were catalyzed into CO intermediates over Fe_3O_4 active sites, followed by carbon chain propagation over Fe_5C_2 active sites. Compared to the results from K-Fe/C, reaction products were evidently influenced with the utilization of H-ZSM-5 (acid sites), especially olefins selectivity. Except that the selectivity of CH_4 (11.1%) was decreased, C_2-C_4 products were changed from olefins (37.9 % for $C_2^=$-$C_4^=$) to saturated hydrocarbons (47.9 % for C_2^0-C_4^0). In addition, C_{2+} olefins approaching 70.0% selectivity were converted into aromatics and saturated hydrocarbons (Figure 2.7 and 2.8). Thereinto, the hydrocarbon products in gasoline-range were mainly isomeric hydrocarbons and aromatic hydrocarbons. By contrast, hydrocarbon products distribution was further shifted toward heavy hydrocarbons from light alkanes (C_3-C_4 products) on K-Fe/C+K-ZSM-5 (Fig. 2.7a). The results revealed that K^+-ion exchange for ZSM-5 was beneficial for the formation of liquid hydrocarbons, approaching 70.1% from the original 39.9% (K-Fe/C+K-ZSM-5 vs. K-Fe/C+H-ZSM-5). According to hydrocarbon products distribution, it could be found that light hydrocarbons selectivity (C_3-C_4) was suppressed and heavy hydrocarbons (C_{5+}) increased obviously (Fig. 2.7a, K-Fe/C+H-ZSM-5). To further verify the promotional effects driven by K^+-ion exchange, sequential exchange strategy (H-type ZSM-5→K-type ZSM-5→H-type ZSM-5) was used to obtain H-ZSM-5* zeolite. As expected, the catalytic behavior on K-Fe/C+H-ZSM-5* deteriorated obviously, and its reaction performance was close to that of the original composite catalyst (K-Fe/C+H-ZSM-5). Apparently, different ion-exchange strategies could significantly affect the selectivity of catalytic products by regulating surface acid properties of ZSM-5. On the contrary, CO_2 conversion and CO selectivity rely on K-Fe/C catalyst rather than zeolites regardless of ion exchange. To

further explore the impacts of ion exchange, various cations were adopted to adjust catalytic performance (Fig. 2.7b). As illustrated, the catalyst with Na^+-ion exchange exhibited a similar performance to the catalyst with K^+-ion exchange modification. C_{5+} selectivity was around at 52% over a catalyst in which the zeolite was treated by one from Mg, Mn, Cu, or Ce ion, which was a little higher than that of K-Fe/C+La-ZSM-5.

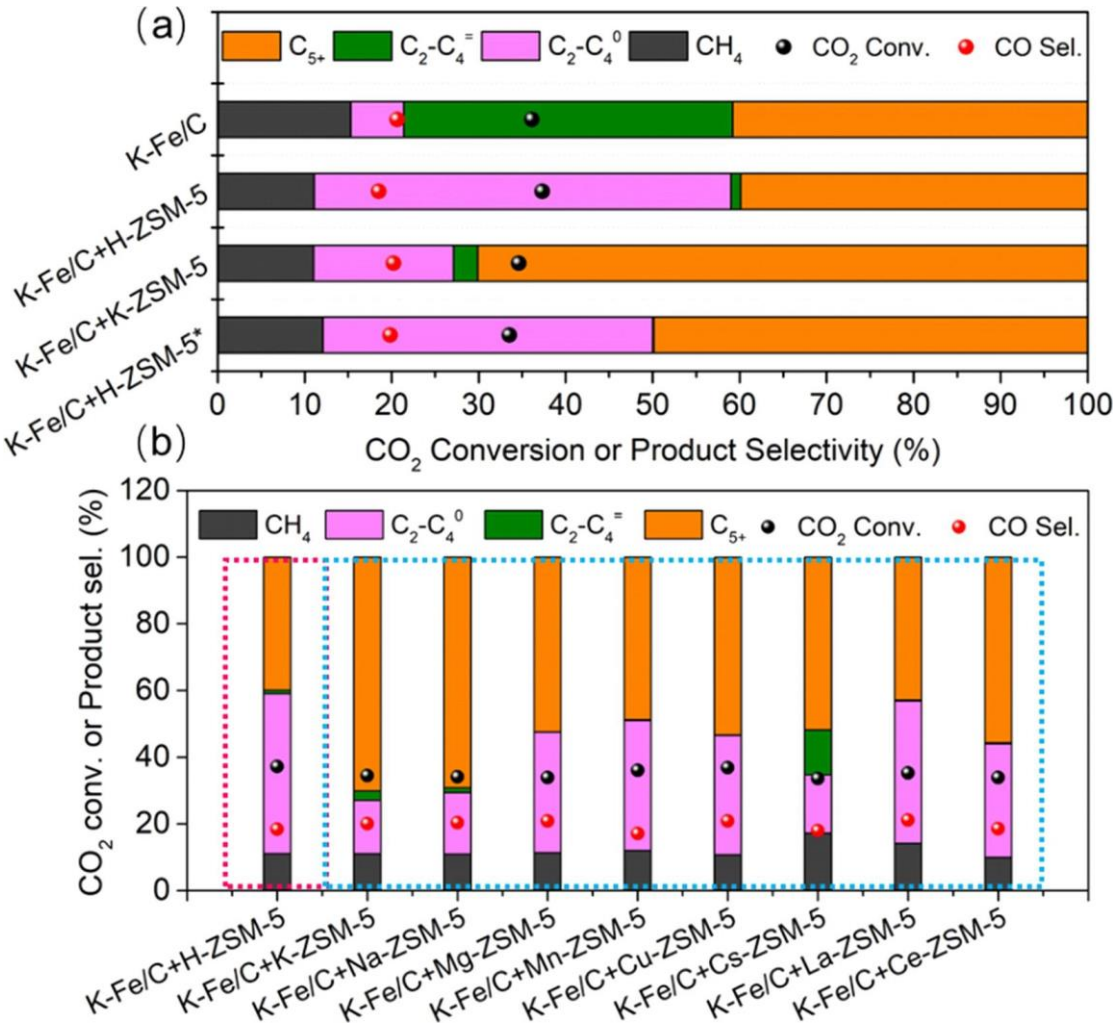

Fig. 2.7. (a) Catalytic performance of different catalysts (K-Fe/C; K-Fe/C+H-ZSM-5; K-Fe/C+K-ZSM-5; K-Fe/C+H-ZSM-5*, H-ZSM-5* stands for K-ZSM-5 treated by NH_4^+ ion-exchange again); (b) Hydrocarbon selectivity over different bifunctional catalysts with various ion-exchange strategies. Reaction conditions: mass ratio of K-Fe/C to zeolite = 1/3, 2.0 MPa, 320 °C, 1200 $mLg^{-1}h^{-1}$ (4800 $mLg^{-1}h^{-1}$ for K-Fe/C), H_2/CO_2 = 2.5. C_2-C_4^0 means paraffins, and C_2-$C_4^=$ means olefins.

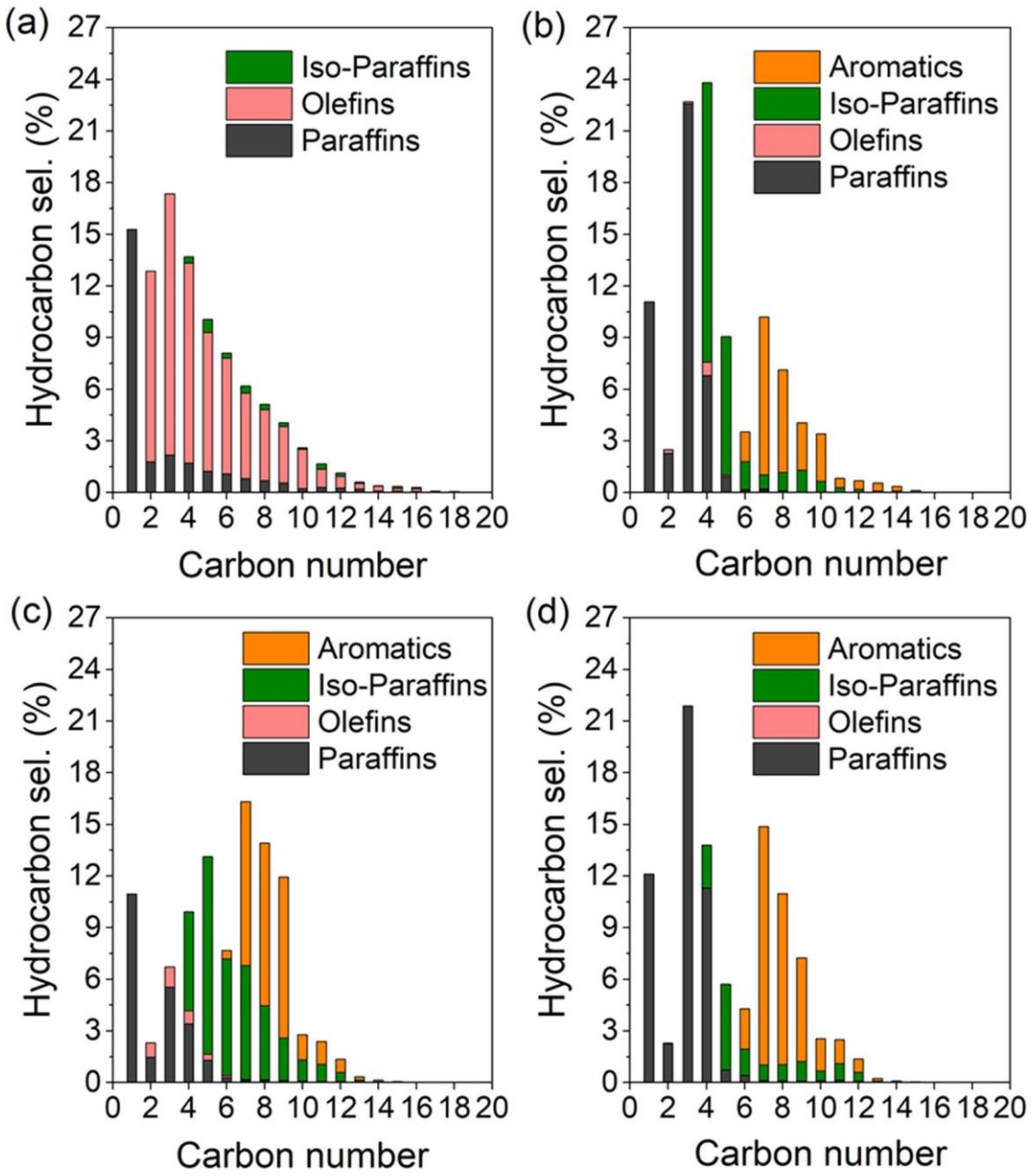

Fig. 2.8. Detailed hydrocarbons distribution over bifunctional catalysts with different ion-exchange strategies for zeolites. (a) K-Fe/C, (b) K-Fe/C+H-ZSM-5, (c) K-Fe/C+K-ZSM-5, (d) K-Fe/C+H-ZSM-5*, Reaction conditions: mass ratio of K-Fe/C to zeolite = 1/3, 2.0 MPa, 320 °C, 1200 $mLg^{-1}h^{-1}$ (4800 $mLg^{-1}h^{-1}$ for K-Fe/C), H_2/CO_2 = 2.5.

Table 2.3. Catalytic performance of CO_2 hydrogenation over different composite catalysts. [a]

Catalysts	CO_2 Conv. (%)	CO Sel. (%)	Hydrocarbons (%)			Olefins Sel. (%) [b]
			CH_4	C_{2-4}	C_{5+}	
K-Fe/C	35.6	20.9	15.3	43.9	40.8	70.0
K-Fe/C-H-ZSM-5	37.2	18.1	11.1	49.0	39.9	1.3
K-Fe/C-K-ZSM-5	34.5	18.8	11.0	18.9	70.1	3.5
K-Fe/C-H-ZSM-5*	33.7	18.3	12.1	38.0	49.9	0.4

[a] Reaction conditions: mass ratio of K-Fe/C to zeolite = 1/3, 2.0 MPa, 320 °C, 1200 $mLg^{-1}h^{-1}$ (4800 $mLg^{-1}h^{-1}$ for K-Fe/C), H_2/CO_2 = 2.5.

[b] Olefins Sel. (%) represents olefins selectivity in whole hydrocarbons.

With the utilization of H-ZSM-5 zeolite, the reaction products were mainly light saturated hydrocarbons (C_3-C_4) and heavy aromatic hydrocarbons (C_6-C_{12}). Different from K-Fe/C+H-ZSM-5 composite catalyst, C_3-C_4 hydrocarbon selectivity was decreased evidently while the selectivity of gasoline (C_5-C_{12}) was increased dramatically over a K-Fe/C+K-ZSM-5 composite catalyst. Combined with Fig. 2.4 and Fig. 2.7a, it could be easily concluded that the catalytic performance was obviously affected by the acid types of zeolite. With the utilization of H-ZSM-5, alkene intermediates underwent oligomerization, isomerization and aromatization at strong acid sites and weak acid sites, and mainly by the over-cracking reaction process to produce C_3-C_4 saturated hydrocarbons. When the K-ZSM-5 was used, alkene intermediates could also undergo oligomerization, isomerization and aromatization reaction at weak acid sites. Mainly isomerization and aromatization reaction occurred rather than over-cracking reaction process. It was obvious that the presence of strong surface acid sites significantly inhibited the formation of high carbon products in this composite catalytic system. Similarly, the selectivity of liquid hydrocarbons was

improved due to the apparent weakening of surface strong acids by Na^+-ion exchange. Although the exchange of other metal ions could change the surface acidity, the relative content of acid-base sites was not changed significantly, thus the catalytic performance was not significantly improved. It was worth noting that because Cs^+-ion exchange significantly reduced the surface acid sites, the olefin intermediates still existed obviously, which indicated that the surface acid sites were the key active sites for the secondary reaction of olefin to liquid fuels. These findings confirmed that the selectivity of liquid hydrocarbon products from CO_2 hydrogenation could be well regulated by simply tuning zeolite acid types.

2.3.4 Impacts of contact manner and catalytic stability

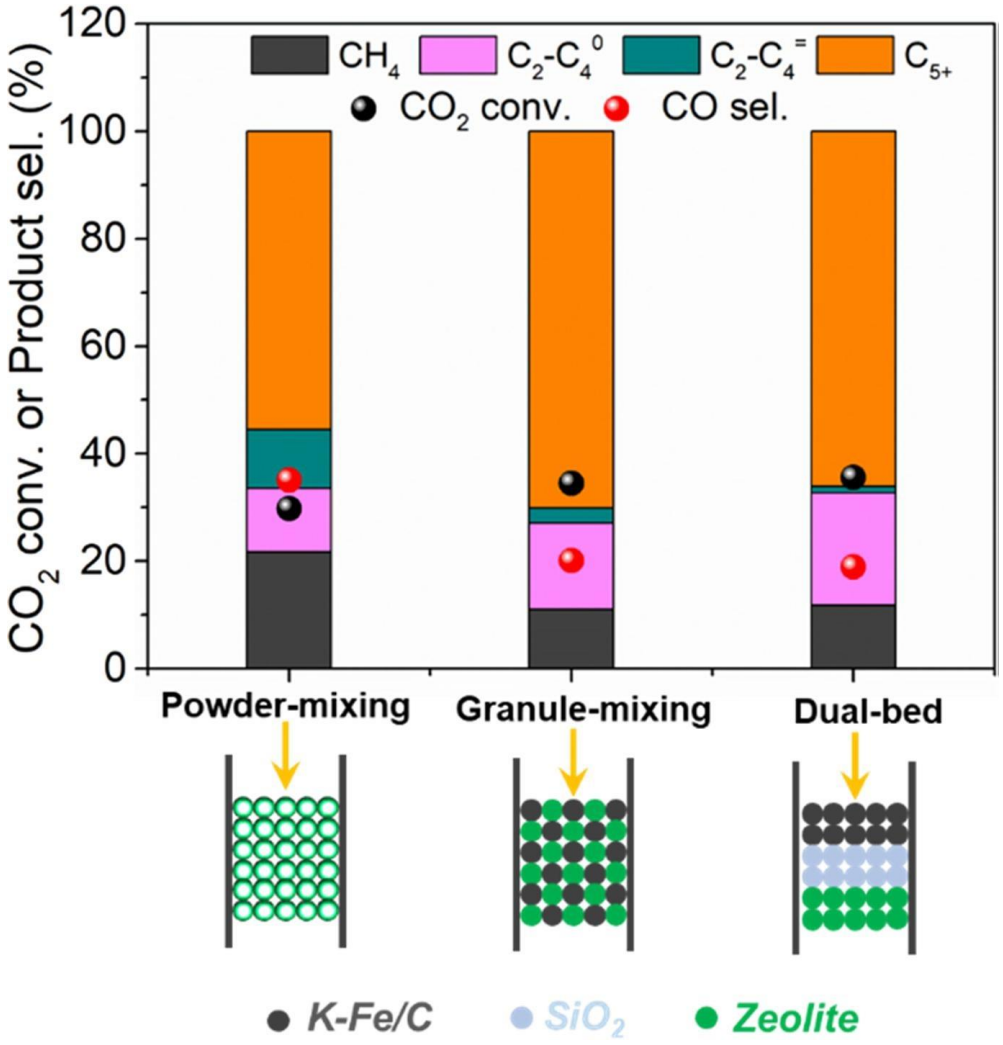

Fig. 2.9 Effects of contacting manner on catalytic performance. Reaction conditions: mass ratio of K-Fe/C to zeolite = 1/3, 2.0 MPa, 320 °C, 1200 $mL g^{-1} h^{-1}$, H_2/CO_2 = 2.5.

Previously, the contacting manner of different active sites in composite catalysts has been reported to exert obvious influence on catalytic activity [9, 11]. Based on this consideration, the contacting manner between F-T catalyst and ZSM-5 catalyst was studied, as shown in Fig. 2.9. When K-Fe/C catalyst and K-ZSM-5 were integrated by powder mixing, the closest proximity between different active sites turned out to be detrimental, exhibiting a low C_{5+} selectivity. This phenomenon might be attributed to that the acidic sites poisoned the alkali K promoter on the K-Fe/C catalyst. By contrary, for a composite catalyst integrated by granule mixing, the distance between active sites was enlarged, and the alkene intermediates formed on K-Fe/C underwent isomerization, aromatization, and oligomerization, presenting a rather high liquid hydrocarbons selectivity (70.1%). With regard to dual-bed configuration, the distance got rather larger, and the catalytic performance was similar to that of a composite catalyst integrated by granule-mixing. These findings indicate that the appropriate distance between different active sites was a crucial role to achieve excellent performance.

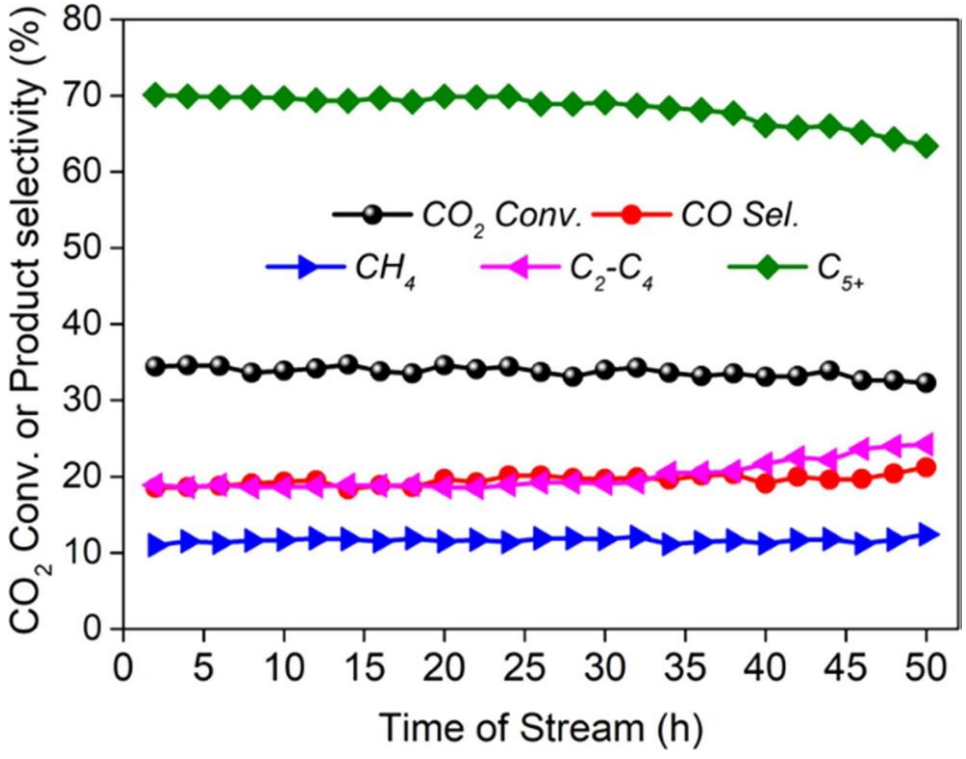

Fig. 2.10 Catalytic stability of K-Fe/C+K-ZSM-5 catalyst. Reaction conditions: mass ratio of K-Fe/C to zeolite = 1/3, 2.0 MPa, 320 °C, 1200 $mLg^{-1}h^{-1}$, H_2/CO_2 = 2.5.

Catalytic stability of the composite catalyst with granule-mixing was investigated and depicted in Fig. 2.10. As seen, the catalyst was able to exhibit a good stability during the initial 40 h. Liquid hydrocarbons selectivity maintained at 70%, and CO_2 conversion as well as un-desired CO byproduct almost kept unchanged. As the reaction time increased from 40 to 50 h, the selectivity of liquid hydrocarbons was decreased slightly, while a high selectivity was still maintained. It indicated that the composite catalyst comprising of K-Fe/C and K-ZSM-5 is a promising catalyst for efficiently catalyzing CO_2 hydrogenation to liquid fuels.

2.3.5 Mechanism analysis on the effect of surface acid properties to catalytic performance

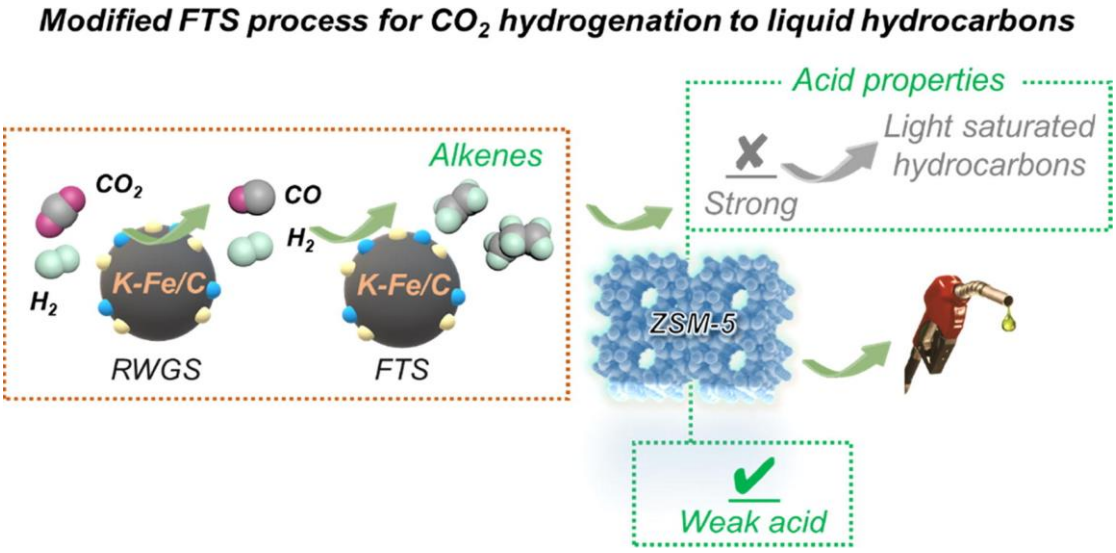

Fig. 2.11 Reaction scheme for CO_2 hydrogenation process regulated by surface acid properties.

The effect of surface acid properties on catalytic performance was depicted in Fig. 2.11. CO_2 feedstock molecules first undergo a conventional F-T synthesis process on the K-Fe/C catalyst to form alkenes (Fe_3O_4 sites for RWGS, followed by Fe_5C_2 for chain propagation) [39]. The generated alkenes initiate secondary reactions over an acid site of ZSM-5, such as oligomerization, isomerization and aromatization [9, 40, 41]. However, the presence of strong acidity of zeolites is able to cause the over-cracking of hydrocarbon products, leading to high selectivity of undesirable light saturated

hydrocarbons (C_{2-4}) [38, 42]. Correspondingly, with the utilization of K^+-ion exchange strategy, the surface strong acid sites are eliminated, which promote the formation of liquid fuels. By contrary, for parent ZSM-5 without any modification, the strong acid sites result in the formation of light saturated hydrocarbons. Thus, facilely regulating surface acid properties of ZSM-5 via a simple ion exchange is a promising means for improving CO_2 hydrogenation performance.

2.4 Conclusion

CO_2 molecules are converted to CO through RWGS reaction over iron oxides, and then abundant primary alkenes are synthesized by the means of FTS process over iron carbide species. The formed alkenes initiate secondary reactions such as isomerization, oligomerization hydrogenation and aromatization reaction over acid sites of ZSM-5, which can be well regulated by ion exchange. The existence of strong acid sites promotes the formation of light products while the existence of weak acid sites facilitates the production of heavy gasoline product. More importantly, alkali K or Na ions, especially K^+ ions, are effective in reducing surface strong acids, boosting up C_{5+} hydrocarbon selectivity. These findings provide new insights for the liquid fuels production from CO_2 hydrogenation over composite catalysts by facilely regulating surface acid properties of zeolite.

References

[1] E.V. Kondratenko, G. Mul, J. Baltrusaitis, G.O. Larrazábalc, J. Pérez-Ramírez, *Energy Environ. Sci.*, 6 (2013) 3112-3135.

[2] R.P. Ye, J. Ding, W. Gong, M.D. Argyle, Q. Zhong, Y. Wang, C.K. Russell, Z. Xu, A.G. Russell, Q. Li, M. Fan, Y.G. Yao, *Nat. Commun.*, 10 (2019) 5698.

[3] C. Hepburn, E. Adlen, J. Beddington, E.A. Carte, S. Fuss, N.M. Dowell, J.C. Minx, P. Smith, C.K. Williams, *Nature*, 575 (2019) 87.

[4] M. Aresta, A. Dibenedetto, A. Angelini, *Chem. Rev.*, 114 (2014) 1709-1742.

[5] W. Wang, S. Wang, X. Ma, J. Gong, *Chem. Soc. Rev.*, 40 (2011) 3703-3727.

[6] L. Guo, J. Sun, Q. Ge, N. Tsubaki, *J. Mater. Chem. A*, 6 (2018) 23244-23262.

[7] H. Yang, C. Zhang, P. Gao, H. Wang, X. Li, L. Zhong, W. Wei, Y. Sun, *Catal. Sci. Technol.*, 7 (2017) 4580-4598.

[8] W. Zhou, K. Cheng, J. Kang, C. Zhou, V. Subramanian, Q. Zhang, Y. Wang, *Chem. Soc. Rev.*, 48 (2019) 3193-3228.

[9] J. Wei, Q. Ge, R. Yao, Z. Wen, C. Fang, L. Guo, H. Xu, J. Sun, *Nat. Commun.*, 8 (2017) 15174-15181.

[10] Y.H. Choi, Y.J. Jang, H. Park, W.Y. Kim, Y.H. Lee, S.H. Choi, J.S. Lee, *Appl. Catal. B-Environ*, 202 (2017) 605-610.

[11] P. Gao, S. Li, X. Bu, S. Dang, Z. Liu, H. Wang, L. Zhong, M. Qiu, C. Yang, J. Cai, W. Wei, Y. Sun, *Nat. Chem.*, 9 (2017) 1019-1024.

[12] R. McGinnis, *Joule*, 4 (2020) 1-3.

[13] Z. He, M. Cui, Q. Qian, J. Zhang, H. Liu, B. Han, *P. Natl. Acad. Sci. USA*, 116 (2019) 12654-12659.

[14] Y.H. Choi, E.C. Ra, E.H. Kim, K.Y. Kim, Y.J. Jang, K.-N. Kang, S.H. Choi, J.H. Jang, J.S. Lee, *ChemSusChem*, 10 (2017) 4764 -4770.

[15] U. Rodemerck, M. Holeña, E. Wagner, Q. Smejkal, A. Barkschat, M. Baerns, *ChemCatChem*, 5 (2013) 1948-1955.

[16] S. Geng, F. Jiang, Y. Xu, X. Liu, *ChemCatChem*, 8 (2016) 1303-1307.

[17] M. Amoyal, R. Vidruk-Nehemya, M.V. Landau, M. Herskowitz, *J. Catal.*, 348 (2017) 29-39.

[18] F. Jiang, B. Liu, S. Geng, Y. Xu, X. Liu, *Catal. Sci. Technol.*, 8 (2018) 4097-4107.

[19] L. Guo, J. Li, R. Kosol, Y. Cui, N. Kodama, X. Guo, R. Prasert, V. Tharapong, G. Liu, J. Wu, G. Yang, Y. Yoneyama, N. Tsubaki, *Fuel*, 276 (2020) 118102.

[20] L. Guo, J. Sun, X. Ji, J. Wei, Z. Wen, R. Yao, H. Xu, Q. Ge, *Commun. Chem.*, 1 (2018) 11.

[21] J. Lu, L. Yang, B. Xu, Q. Wu, D. Zhang, S. Yuan, Y. Zhai, X. Wang, Y. Fan, Z. Hu, *ACS Catal.*, 4 (2014) 613-621.

[22] L. Guo, J. Li, Y. Cui, R. Kosol, Y. Zeng, G. Liu, J. Wu, T. Zhao, G. Yang, L. Shao, P. Zhan, J. Chen, N. Tsubaki, *Chem. Comm.*, 56 (2020) 9372-9375.

[23] Y. Wang, L. Tan, M.H. Tan, P.P. Zhang, Y. Fang, Y. Yoneyama, G.H. Yang, N. Tsubaki, *ACS Catal.*, 9 (2019) 895-901.

[24] Z. Li, J. Wang, Y. Qu, H. Liu, C. Tang, S. Miao, Z. Feng, H. An, C. Li, *ACS Catal.*, 7 (2017) 8544-8548.

[25] X. Liu, M. Wang, C. Zhou, W. Zhou, K. Cheng, J. Kang, Q. Zhang, W. Deng, Y. Wang, *Chem. Commun.*, 54 (2018) 140-143.

[26] J. Zhang, M. Zhang, S. Chen, X. Wang, Z. Zhou, Y. Wu, T. Zhang, G. Yang, Y. Han, Y. Tan, *Chem. Comm.*, 55 (2019) 973-976.

[27] Z. Li, Y. Qu, J. Wang, H. Liu, M. Li, S. Miao, C. Li, *Joule*, 3 (2019) 570-583.

[28] C. Zhou, J. Shi, W. Zhou, K. Cheng, Q. Zhang, J. Kang, Y. Wang, *ACS Catal.*, 10 (2020) 302-310.

[29] P. Gao, S. Dang, S. Li, X. Bu, Z. Liu, M. Qiu, C. Yang, H. Wang, L. Zhong, Y. Han, Q. Liu, W. Wei, Y. Sun, *ACS Catal.*, 8 (2017) 571-578.

[30] J. Ye, C. Liu, D. Mei, Q. Ge, *ACS Catal.*, 3 (2013) 1296-1306.

[31] J. Wei, R. Yao, Q. Ge, Z. Wen, X. Ji, C. Fang, J. Zhang, H. Xu, J. Sun, *ACS Catal.*, 8 (2018) 9958-9967.

[32] Y.B. Xu, C.M. Shi, B. Liu, T. Wang, J. Zheng, W.P. Li, D.P. Liu, X.H. Liu, *Catal. Sci. Technol.*, 9 (2019) 593-610.

[33] L. Tan, P. Zhang, Y. Cui, Y. Suzuki, H. Li, L. Guo, G. Yang, N. Tsubaki, *Fuel. Process. Technol.*, 196 (2019) 106174.

[34] L. Guo, P. Zhang, Y. Cui, G. Liu, J. Wu, G. Yang, Y. Yoneyama, N. Tsubaki, *ACS Sustainable Chem. Eng.*, 7 (2019) 8331-8339.

[35] L. Guo, J. Sun, J. Wei, Z. Wen, H. Xu, Q. Ge, *J. Energy Chem.*, 26 (2017) 632-638.

[36] J. Li, Y. He, L. Tan, P. Zhang, A. Oruganti, G. Yang, H. Abe, Y. Wang, N. Tsubaki, *Nat. Catal.*, 1 (2018) 787-793.

[37] N. Katada, H. Igi, J.-H. Kim, M. Niwa, *J. Phys. Chem. B*, 101 (1997) 5969-5977.

[38] J. Kang, K. Cheng, L. Zhang, Q. Zhang, J. Ding, W. Hua, Y. Lou, Q. Zhai, Y. Wang, *Angew. Chem. Int. Ed.*, 50 (2011) 5200-5203.

[39] B. Liang, T. Sun, J. Ma, H. Duan, L. Li, X. Yang, Y. Zhang, X. Su, Y. Huang, T. Zhao, *Catal. Sci. Technol.*, 9 (2019) 456-464.

[40] A. Noreen, M. Li, Y. Fu, C. Cyril Amoo, J. Wang, E. Maturura, C. Du, R. Yang, C. Xing, J. Sun, *ACS Catal.*, 2020, 10, 14186-14194.

[41] J. Plana-Pallejà, S. Abelló, C. Berrueco, D. Montané, *Appl. Catal. A*, 515 (2016) 126-135.

[42] C. Liu, Y. Chen, Y. Zhao, S. Lyu, L. Wei, X. Li, Y. Zhang, J. Li, *Fuel*, 263 (2020) 116619.

Summary

Against the backdrop of the global warming and ocean acidification, carbon neutrality becomes the common goal of all mankind. Being an integral part for achieving global carbon neutrality, the reutilization of CO_2 recently attracts much attention. Among various techniques, catalytic hydrogenating CO_2 into carbon neutral liquid fuels via a modified CO_2-FTS route is a promising and powerful way to reduce the consumption of fossil fuels and simultaneously solve the environmental problems. In this route, Fe-based catalysts, which are regarded as conventional FTS catalysts, have been extensively used. Unfortunately, pure Fe catalyst generally exhibits low CO_2 conversion and high selectivity of undesirable products. Therefore, many efforts have been focused on optimizing preparation method and composition of the catalysts, as well as reaction conditions, for clarifying the relationship between excellent catalytic performances and reaction mechanisms. As discussed in the current thesis, various promoters, including K, Mn, Ti and acidic zeolites, have been incorporated into Fe catalyst for breaking the limitation of ASF model and improving the yield of C_{5+} hydrocarbons.

In chapter 1, multi-promoters were incorporated into Fe catalyst by co-precipitation method and impregnation method. After the addition of K, competitive adsorption of H_2 and CO_2 was enhanced, resulting in that less H_2 could participate in the reaction, which is beneficial to the chain growth of hydrocarbons. Besides, more Fe^{2+} and oxygen vacancies formed, leading to the excellent activity of RWGS reaction. Therefore, the K_3/Fe catalyst showed high selectivities of CO and C_{5+}. As for Mn modified catalysts, the formation of iron carbides (active sites for FTS) was promoted by the interaction between Mn and Fe, resulting in the rapid consumption of CO (low CO selectivity). With the addition of Ti, CO_2 adsorption ability and pore structure of catalysts were promoted, leading to the high CO_2 conversion and C_{5+} selectivity. In order to further regulate the relationship between RWGS and FTS, the contents of each promoter were regulated. The results showed that addition of excessive promoter led to

the suppression of Fe oxidation-reduction (K) and the decreased of total active metal content (Mn and Ti). As a result, the well-matching catalysis between RWGS and FTS was achieved over the $K_3/Fe_{90}Mn_{10}Ti_{20}$ catalyst with an excellent stability for 50 h. After regulating the reaction conditions, an ultra-high yield of C_{5+} hydrocarbons (1282.7 $g_{fuel}kg_{cat}^{-1}h^{-1}$) was achieved.

In chapter 2, modified ZSM-5 zeolites were employed to regulate the hydrocarbons distribution of a traditional K-Fe/C catalyst. The physical-chemical properties of K-Fe/C catalyst were firstly studied by various characterizations and found that the active sites for both RWGS (Fe_3O_4) and FTS (Fe_5C_2) reactions could be converted from $FeC_2O_4 \cdot 2H_2O$ during CO_2 hydrogenation. Then, different metal ions (K^+, La^{3+}, Na^+, Cu^{2+}, Mn^{2+}, Mg^{2+}, Ce^{3+}, and Cs^+) were adopted to tune the microenvironment properties of H-ZSM-5 by ion-exchange strategy. Obviously, the pore structure and crystal structure were changed slightly. Differently, the surface acid properties of ZSM-5 were successfully regulated by different ion-exchange strategies, especially K-ZSM-5. Strong acid was visibly eliminated with the treatment of K^+. Due to the weakened strong acids, alkene intermediates mainly underwent oligomerization, isomerization and aromatization (K-ZSM-5) rather than over-cracking reaction process (H-ZSM-5), resulting in the high selectivity of C_{5+} hydrocarbons. As for other ion-exchanged ZSM-5 zeolites, various catalytic performances were found, indicating that the selectivity of C_{5+} hydrocarbons could be well regulated by simply tuning zeolite acid types. In addition, the contacting manner between FTS catalyst (K-Fe/C) and zeolite catalyst (K-ZSM-5) was studied. When the composite catalyst was integrated by granule mixing, the suitable distance between active sites promoted the formation of C_{5+} hydrocarbons, presenting a high C_{5+} selectivity of 70.1 % and a well stability of 50 h.

These findings provide new insights in the modification measure of catalysts for the carbon neutral liquid fuel production from CO_2 hydrogenation, including regulating the relationship between RWGS and FTS reaction, and tuning the surface acidity of catalysts. Meanwhile, these work pushes the process of global carbon neutrality forward.

List of publications

[1] **Heng Zhao**, Lisheng Guo, Weizhe Gao, Fei Chen, Xuemei Wu, Kangzhou Wang, Yingluo He, Peipei Zhang, Guohui Yang, Noritatsu Tsubaki, Multi-Promoters Regulated Iron Catalyst with Well-Matching Reverse Water-Gas Shift and Chain Propagation for Boosting CO_2 Hydrogenation, *Journal of CO_2 Utilization*, 52 (2021): 101700.

[2] Lisheng Guo, Song Sun, Jie Li, Weizhe Gao, **Heng Zhao**, Baizhang Zhang, Yingluo He, Peipei Zhang, Guohui Yang, Noritatsu Tsubaki, Boosting liquid hydrocarbons selectivity from CO_2 hydrogenation by facilely tailoring surface acid properties of zeolite via a modified Fischer-Tropsch synthesis, *Fuel*, 306 (2021): 121684.

[3] **Heng Zhao**, Chunyang Zeng, Noritatsu Tsubaki, A mini review on recent advances in thermocatalytic hydrogenation of carbon dioxide to value-added chemicals and fuels, *Resources Chemicals and Materials*, 1 (2022): 230-248.

[4] Yuan Fang, **Heng Zhao**, Xiaoyu Guo, Yingluo He, Guohui Yang, Noritatsu Tsubaki, Silicalite-1 encapsulated rhodium nanoparticles for hydroformylation of 1-hexene, Catalysis Today, https://doi.org/10.1016/j.cattod.2022.05.029.

[5] Fei Chen, Weizhe Gao, Baizhang Zhang, **Heng Zhao**, Liwei Xiao, Yuya Araki, Xiaojing Yong, Wei Zhang, Tiejian Zhao, Zhongshan Guo, Yingluo He, Peipei Zhang, Noritatsu Tsubaki, Effect of Different Chelating Agents on the Physicochemical Properties of Cu/ZnO Catalysts for Low-temperature Methanol Synthesis from Syngas Containing CO_2, *Journal of the Japan Petroleum Institute*, 64 (2021): 245-255.

[6] Kangzhou Wang, Xiaobo Peng, Xinhua Gao, Yuya Araki, **Heng Zhao**, Jiaming Liang, Liwei Xiao, Jienan Chen, Guangbo Liu, Jinhu Wu, Guohui Yang, Noritatsu Tsubaki, Insights into the synergistic effect of active centers over ZnMg/SBA-15 catalysts in direct synthesis of butadiene from ethanol, *Reaction Chemistry & Engineering*, 6 (2021): 548-558.

[7] Yu Cui, Lisheng Guo, Weizhe Gao, Kangzhou Wang, **Heng Zhao**, Yingluo He, Peipei Zhang, Guohui Yang, Noritatsu Tsubaki, From Single Metal to Bimetallic Sites: Enhanced Higher Hydrocarbons Yield of CO_2 Hydrogenation over Bimetallic Catalysts, *ChemistrySelect*, 6 (2021): 5241-524.

[8] Kangzhou Wang, Lisheng Guo, Weizhe Gao, Baizhang Zhang, **Heng Zhao**, Jiaming Liang, Na Liu, Yingluo He, Peipei Zhang, Guohui Yang, Noritatsu Tsubaki, One-Pot Hydrothermal Synthesis of Multifunctional ZnZrTUD-1 Catalysts for Highly Efficient Direct Synthesis of Butadiene from Ethanol, *ACS Sustainable chemistry & Engineering*, 9 (2021): 10569-10578.

[9] Yang Wang, Weizhe Gao, Kangzhou Wang, Xinhua Gao, Baizhang Zhang, **Heng Zhao**, Qingxiang Ma, Peipei Zhang, Guohui Yang, Mingbo Wu, Noritatsu Tsubaki, Boosting the synthesis of value-added aromatics directly from syngas via a Cr_2O_3 and Ga doped zeolite capsule catalyst, *Chemical Science*, 12 (2021): 7786-7792.

[10] Fei Chen, Peipei Zhang, Liwei Xiao, Jiaming Liang, Baizhang Zhang, **Heng Zhao**, Rungtiwa Kosol, Qingxiang Ma, Jienan Chen, Xiaobo Peng, Guohui Yang, Noritatsu Tsubaki, Structure-Performance Correlations over Cu/ZnO Interface for Low-Temperature Methanol Synthesis from Syngas Containing CO_2, *ACS Applied Materials & Interfaces*, 13 (2021): 8191-8205.

[11] Faen Song, Xiaojing Yong, Xuemei Wu, Wei Zhang, Qingxiang Ma, Tiejian Zhao, Minghui Tan, Zhongshan Guo, **Heng Zhao**, Guohui Yang, Noritatsu Tsubaki, Yisheng Tan, FeMn@HZSM-5 capsule catalyst for light olefins direct synthesis via Fischer-Tropsch synthesis: Studies on depressing the CO_2 formation, *Applied Catalysis B: Environmental*, 300 (2022): 120713.

List of conferences

1. **Heng Zhao**, Yingluo He, Guohui Yang, Noritatsu Tsubaki, Ultra-high yield coproduction of C_{5+} hydrocarbons and ethanol from CO_2 hydrogenation on a rational designed multi-functional catalyst. *12th International Conference on Environmental Catalysis*, Osaka, Japan, July 30-August 2, 2022, *Poster (Virtual)*.
2. **Heng Zhao**, Guohui Yang, Noritatsu Tsubaki, Multi-promoters regulated iron catalyst with well-matching reverse water-gas shift and chain propagation for boosting CO_2 hydrogenation, *The 9th Tokyo Conference on Advanced Catalytic Science and Technology*, Fukuoka, Japan, July 24-29, 2022, *Oral*.
3. **Heng Zhao**, Guohui Yang, Noritatsu Tsubaki, Insight into the effect of oxygen species and Mn chemical valence over MnO_x on the catalytic oxidation of toluene. *The 2021 International Chemical Congress of Pacific Basin Societies*, Hawaii, USA, December 16-21, 2021, *Poster (Virtual)*.
4. **Heng Zhao**, Guohui Yang, Yoshiharu Yoneyama, Noritatsu Tsubaki, Insight into the effect of oxygen species and Mn chemical valence over MnO_x on the catalytic oxidation of toluene. *18th Japan-Korea Symposium on Catalysis*, Osaka, November 23-25, 2021, *Poster (Virtual)*.
5. **Heng Zhao**, Guohui Yang, Noritatsu Tsubaki, Insight into the effect of oxygen species and Mn chemical valence over MnO_x on the catalytic oxidation of toluene. *51st Petroleum-Petrochemical Symposium of JPI*, Hakodate, November 11-12, 2021, *Oral*.

Acknowledgments

The three-year doctoral life has gone in a flash, and I feel very fulfilled when I recall the past years. As the dissertation is about to be completed, I have a lot of feelings.

First of all, I would like to express my sincere thanks to my supervisor, Professor Noritatsu Tsubaki, for his hard work and help in the process of establishing the thesis, the experimental process and the final paper. With his rigorous academic attitude, generous and kind-hearted mind, and positive and optimistic attitude towards life, my teacher has set an example for my lifelong learning. His teaching and encouragement will encourage me to make great efforts and pioneering innovation on the road of research and teaching.

At the same time, I would like to express my heartfelt thanks to Associate Professor Guohui Yang for his help and valuable guidance in my study. His erudition about science not only inspired my study during the Ph.D., but also inspired my future study and life.

My sincere thanks also go to members in Tsubaki lab for offering me a lot of help in my experiment and life. They are Dr. Xiaobo Peng, Dr. Peipei Zhang, Dr. Yingluo He, Dr. Yang Wang, Dr. Hangjie Li, Dr. Lisheng Guo, Dr. Yuan Fang, Dr. Xiaoyu Guo, Dr. Yan Zeng, Dr. Kangzhou Wang, Ms. Na Liu, Mr. Weizhe Gao, Mr. Yu Cui, Mr. Baizhang Zhang, Mr. Jie Yao, Mr. Fei Chen, Mr. Jiaming Liang, Mr. Chenwei Wang, Mr. Jiaqi Fan, Mr. Liwei Xiao, Ms. Xuemei Wu and many other Japanese students.

Finally, thanks to my parents and my beloved for their continued encouragement and spiritual support during my PhD period. I would like to express my sincere thanks to the financial support of JST SPRING, Grant Number JPMJSP2145.